In vivo ectopic Ngn1 and Neurod1 convert neonatal cochlear glial cells into spiral ganglion neurons

Article *in* The FASEB Journal · February 2020

DOI: 10.1096/fj.201902118R

6 authors, including:

Chao Li
Shanghai Institutes for Biological Sciences
26 PUBLICATIONS **193** CITATIONS
SEE PROFILE

Zhiyong Liu
Institute of Neuroscience
26 PUBLICATIONS **824** CITATIONS
SEE PROFILE

Received: 20 August 2019 | Revised: 14 January 2020 | Accepted: 22 January 2020

DOI: 10.1096/fj.201902118R

RESEARCH ARTICLE

THE FASEB JOURNAL

In vivo ectopic Ngn1 and Neurod1 convert neonatal cochlear glial cells into spiral ganglion neurons

Xiang Li[1] | **Zhenghong Bi**[1] | **Yidi Sun**[2,3] | **Chao Li**[1] | **Yixue Li**[3,4] | **Zhiyong Liu**[1,5]

[1]Institute of Neuroscience, State Key Laboratory of Neuroscience, CAS Center for Excellence in Brain Science and Intelligence Technology, Chinese Academy of Sciences, Shanghai, China

[2]CAS Key Laboratory of Systems Biology, CAS Center for Excellence in Molecular Cell Science, Institute of Biochemistry and Cell Biology, Shanghai Institutes for Biological Sciences, Chinese Academy of Sciences, Shanghai, China

[3]University of Chinese Academy of Sciences, Shanghai, China

[4]Bio-Med Big Data Center, Key Laboratory of Computational Biology, CAS-MPG Partner Institute for Computational Biology, Shanghai Institute of Nutrition and Health, Shanghai Institutes for Biological Sciences, Chinese Academy of Sciences, Shanghai, China

[5]Shanghai Center for Brain Science and Brain-Inspired Intelligence Technology, Shanghai, China

Correspondence
Zhiyong Liu, Institute of Neuroscience, State Key Laboratory of Neuroscience, CAS Center for Excellence in Brain Science and Intelligence Technology, Chinese Academy of Sciences, Shanghai 200031, China.
Email: Zhiyongliu@ion.ac.cn

Funding information
Ministry of Science and Technology of the People's Republic of China (MOST), Grant/Award Number: 2017YFA0103901; Chinese Academy of Sciences (CAS), Grant/Award Number: XDB32060100; National Natural Science Foundation of China (NSFC), Grant/Award Number: 81771012; Science and Technology Commission of Shanghai Municipality (STCSM), Grant/Award Number: 2018SHZDZX05; Boehringer Ingelheim, Grant/Award Number: DE811138149

Abstract

Damage or degeneration of inner ear spiral ganglion neurons (SGNs) causes hearing impairment. Previous in vitro studies indicate that cochlear glial cells can be reprogrammed into SGNs, however, it remains unknown whether this can occur in vivo. Here, we show that neonatal glial cells can be converted, in vivo, into SGNs (defined as new SGNs) by simultaneous induction of *Neurog1 (Ngn1)* and *Neurod1*. New SGNs express SGN markers, *Tuj1, Map2, Prox1, Mafb* and *Gata3*, and reduce glial cell marker *Sox10* and *Scn7a*. The heterogeneity within new SGNs is illustrated by immunostaining and transcriptomic assays. Transcriptomes analysis indicates that well reprogrammed SGNs are similar to type I SGNs. In addition, reprogramming efficiency is positively correlated with the dosage of Ngn1 and Neurod1, but declined with aging. Taken together, our in vivo data demonstrates the plasticity of cochlear neonatal glial cells and the capacity of Ngn1 and Neurod1 to reprogram glial cells into SGNs. Looking ahead, we expect that combination of Neurog1 and Neurod1 along with other factors will further boost the percentage of fully converted (Mafb+/Gata3+) new SGNs.

KEYWORDS

cochlea, glial cells, inner ear, *Neurog1*, *Neurod1*, regeneration, spiral ganglion neurons

1 | INTRODUCTION

Our auditory organ, the cochlea, resides in the ventral portion of the inner ear. The cochlear auditory epithelium, also referred as to organ of Corti,[1] consists of two types of auditory hair cells (HCs), inner hair cells (IHCs) and outer hair cells (OHCs), and neighboring supporting cells (SCs). The OHCs detect and amplify sound; this subsequently leads to the activation

Abbreviations: BDNF, brain-derived neurotrophic factor; DT, diphtheria toxin; DTR, diphtheria toxin receptor; HC, hair cell; IHC, inner hair cell; LSL, Loxp-stop-Loxp; NT-3, neurotrophin-3; OHC, outer hair cell; Plp1, proteolipid protein 1; SC, supporting cell; SGN, spiral ganglion neuron; TPM, transcript per million.

Xiang Li and Zhenghong Bi contributed equally to the work.

Correction added on February 24, 2020, after first online publication: "Neonatal" was added to describe the glial cells in several places and labeling in Figure 3 was corrected to make the arrows easier to see.

of IHCs, which in turn convert sound into electrical signals.[2] Approximately 95% of spiral ganglion neuron (SGNs) are type I SGNs, which can be further subdivided into three subtypes: Type I-A, Type I-B, and Type I-C, and the remaining 5% of SGNs are type II SGNs, as supported by both morphological and single-cell transcriptome analysis.[3-6] IHCs are the primary sensory cells that are connected to myelinated type I SGNs, while OHCs are innervated by unmyelinated type II SGNs. The primary role of type I SGNs is to transmit sound-induced electrical signals from IHCs to the cochlear nucleus located in the brainstem; in contrast type II SGNs are involved in the reflexive medial olivocochlear suppression of cochlear amplification.[7] Degeneration of SGNs can occur as a direct consequence of exposure to large sounds, infection or aging, to name only a few causes, or as a secondary effect of damaging auditory HCs which provide neurotrophic support to SGNs.[8]

Degeneration of SGNs causes permanent hearing impairment as they have no intrinsic regenerative capacity.[9] Understanding how to preserve and/or regenerate SGNs is of growing clinical importance as the demand for cochlear implant or hearing aids is increasing with the aging population and their success critically depends on having functional SGNs cells to relay auditory information to the brain. In the case of partial damage to SGNs, ectopic neurotrophic factors such as brain-derived neurotrophic factor (BDNF) and neurotrophin-3 (NT-3) can protect the remaining cells.[10] In the case of severe loss of SGNs, cell transplantation of otic neuroprogenitors derived from human embryonic stem cells can partially rescue deafness in the ouabain-mediated neuropathic gerbil model.[11,12] However, transplanting stem/progenitor cells into adult cochlea is technically challenging and is accompanied by the risk of tumor formation.[13] An alternative solution is in situ regeneration, which involves reprogramming cochlear glial cells, which surround SGNs, into neuronal lineages. A similar approach has been successful in regenerating neurons from glial cells in the mouse cortex.[14] Recently, isolated cochlear glial cells were converted in vitro into SGNs via the induction of *Ascl1* and/or *Neurod1*.[15] Nonetheless, it remains unknown whether this is possible in vivo.

We addressed this question by inducing ectopic *Neurog1 (Ngn1)* and *Neurod1* in neonatal cochlear glial cells in vivo. Our lineage tracing analysis showed that neonatal glial cells started to express the SGN markers, Tuj1, Map2, and Prox1, as early as 6 days after expressing Ngn1 and Neurod1; we defined these cells as "glial cell-derived new SGNs" or "new SGNs" for short. We found that not all neonatal glia cells with Ngn1 and Neurod1 expression became new SGNs, consistent with previous glial cells to neuron conversion studies in retina.[16,17] Promisingly, the new SGNs also decreased expression of glial genes and could survive at least until 6 weeks of age. More importantly, a smaller subset of new SGNs expressed Mafb, Gata3, and other SGN genes and displayed large rounded somas similar to that of wild-type SGNs. Our transcriptomic analysis showed that Mafb+/Gata3+ new SGNs resembled type I SGNs and that in general two copies of *Ngn1* and *Neurod1* resulted in higher efficiency of cellular reprogramming.

2 | MATERIALS AND METHODS

2.1 | Animals

The *Rosa26-LSL-Ngn1-Neurod1/+* mouse was generated by CRISPR/Cas9-mediated gene targeting in mouse zygotes. The sequence used (without PAM) for the sgRNA in Rosa26 locus (Figure 1A) was: 5′-*AAGGCCGCACCCTTCTCCGG*-3′. The cDNA sequences of *Ngn1* (gene ID: 18014) and *Neurod1* (gene ID: 18012) used were identical to ENSMUST00000058475.5 and ENSMUST00000041099.4, respectively, on the ensembl website (www.ensembl.org). Donor vector DNA (Figure 1B) together with Cas9 and sgRNA were injected into C57BL/6 mouse zygotes. Detailed donor DNA sequences are available upon request. Founder F0 mice were mosaic and screened by junction PCR. The positive F0 mice were crossed with wild-type C57BL/6 mice for germline transition and generating stable F1 mice. F1 mice derived from positive F0 founders were further screened by junction PCR and southern blot analysis (Figure 1D,E). The southern blot confirmed that there was no random insertion of donor DNA in the mice's genomes. Southern blot was performed according to our previously described protocol.[2]

For routine genotype analysis of F2 or later mouse progeny, PCR was performed on mouse tail DNA with the following three primers (used simultaneously) (Figure 1): F1: 5′-*AGTCGCTCTGAGTTGTTATCAG*-3′; R1: 5-*AGTCCCTATTGGCGTTACTATGG*-3′; R2: 5′-*TGAGCATGTCTTTAATCTACCTCGATG*-3′. The PCR amplicon derived from primer F1 and R2 in wild type was 469 bp and 7464 bp in knock-in (KI) allele. 7464 bp was too long to be amplified using our PCR protocol. PCR amplicon of primer F1 and R1 was only present in KI allele with a length of 268 bp. The PCR condition for each cycle was the following: (1) 95°C −5min; (2) 95°C −30sec, 62°C −30sec, 72°C −35 seconds with 35 cycles; (3) 72°C −10 minutes.

The proteolipid protein 1(*Plp1)-CreER+* mouse strain (Jax#: 005975) came from the Jackson laboratory. The Ai47 Cre reporter mouse, *Rosa26-CAG-LSL-3xEGFP,* was requested from Dr Zilong Qiu from the Institute of Neuroscience (ION), CAS. The "3xEGFP" refers to three DNA elements coding for different EGFPs: Emerald-GFP (EmGFP), TagGFP2, and humanized Renilla-GFP (hrGFP). These were connected via the 2A method, as described in one previous study.[18] All mice were maintained according to guidelines of the IACUC of Institute of Neuroscience (ION), Chinese Academy of Sciences. Mice of either sex were used for the experiments.

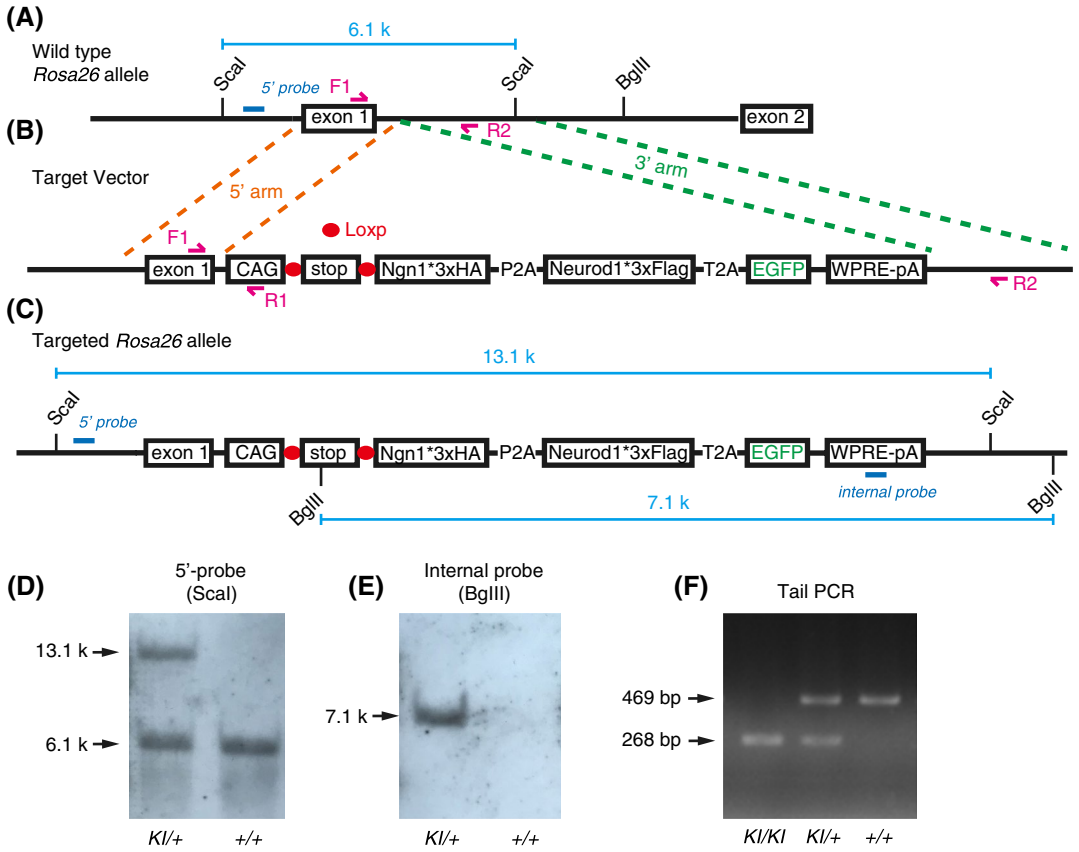

FIGURE 1 Generation of *Rosa26-LSL-Ngn1-Neurod1/+* mouse strain. A-C, Illustration of wild-type Rosa26 locus (A), gene targeting vector (B), and Rosa26 locus post gene targeting (C). Ngn1 was tagged with 3xHA and Neurod1 with 3xFlag at their C-terminus. Ngn1 and Neurod1 cannot be expressed unless the stop fragment is removed by Cre. D-E, Southern Blot analysis using tail genome DNA extracted from F1 mice with 5′-probe outside of 5′-arm (D) and internal probe within WPRE sequences (E). F, PCR genotyping on tail DNA was performed using three mixed primers F1, R1, and R2. The size of knock-in (KI) allele was 268 bp, and wild type (+) was 469 bp. *KI/ KI*: homozygous, *KI/+*: heterozygous, *+/+*: wild type

2.2 | Sample processing, histology, and immunofluorescence

All mice were given tamoxifen (T5648, Sigma) dissolved in corn oil (C8267, Sigma) at P0 and P1, or at P14 and P15, with a 24 hours interval. Tamoxifen dosage was 3mg/40g of mouse body weight. Mice were heart-perfused with 1xPBS followed by a perfusion with fresh 4% PFA. Inner ear tissues were dissected out and further fixed in 4% PFA at 4°C overnight, followed by 1xPBS wash, repeated three times and decalcified with EDTA. After that, they were soaked in 30% sucrose at 4°C overnight and embedded in OCT for cryo-sections with 14μm thickness. Inner ear samples which contained all three cochlear turns were chosen for immunostaining; this aided in determining the exact location of the SGNs when we analyzed samples.

The following primary antibodies were used: anti-GFP (chicken, 1:1000, ab13970, abcam), anti-Tuj1 (mouse, 1:500, 801201, BioLegend), anti-Prox1 (rabbit, 1:500, AB5475, Millipore), Anti-Map2 (rabbit, 1:400, M3696, Sigma), Anti-Mbp (mouse, 1:200, ab62631, abcam), anti-Mafb (rabbit, 1:300, HPA005653, Sigma), anti-Gata3 (goat, 1:200, AF2605, R&D systems), anti-Sox10 (goat, 1:200, sc-17342, Santa Cruz Biotechnology), anti-HA (rat, 1:200, 11867423001, Sigma), anti-Neurod1 (goat, 1:200, sc-1084, Santa Cruz Biotechnology). All secondary antibodies were purchased either from Thermo Scientific or Jackon ImmunoResearch Laboratory. Finally, samples were counter stained with Hoechst33342 (1:1000, 62249, Thermo Scientific) solution in 1xPBS to visualize nuclei and were mounted with Prolong gold anti-fade mounting medium (P36930, Thermo Scientific). All images were captured using Nikon NiE-A1 plus or Nikon C2 confocal microscope, and analyzed using Image J. For detailed inner ear histology protocol, please refer to our previous study.[19]

2.3 | Quantification and statistical analysis of the new SGN populations

Inner ear cryo-section slices with all three cochlear turns were chosen for analysis; we focused on the middle or apical SGN regions where more new SGNs were observed.

Approximately, six good slices with all three cochlear turns were obtained per mouse. The field of view of the confocal microscope (60× objective lens) was sufficiently large to cover most of the SGN area per turn. The samples were scanned in z-stack mode every 0.6 μm. For each mouse (either left or right ears were analyzed), the total number of EGFP+ cells was normalized to total number of SGN regions (5 ~ 8) scanned to calculate an average number of EGFP+ cells (regardless of cell fate). Similar approaches were used to quantify the percentage of new SGNs (using different neuronal markers) among the EGFP+ cells. Note that we did observe EGFP+ new SGNs in SGN regions of basal turn but with a lower frequency. All cell numbers were presented as Mean ± SEM. Cell counts were compared by a one-way ANOVA, followed by a Student's *t* test with a Bonferroni correction. GraphPad Prism 6.0 was used for all statistical analyses.

2.4 | Manual cell picking, qPCR and RNA-Seq library construction

Manual cell picking was used for all three different mouse models. For wild-type glial cells, *Plp1-CreER+ ; Rosa26-CAG-LSL-3xEGFP/+* mice were used. For new SGNs, both *Plp1-CreER+; Rosa26-LSL-Ngn1-Neurod1/+* and *Plp1-CreER+; Rosa26-LSL-Ngn1-Neurod1/ Rosa26-LSL-Ngn1-Neurod1* were used. All models were given tamoxifen at P0 and P1, and samples were dissected and digested at P16. Detailed cell picking protocol can be found in our previous study.[2] Approximately 25 ~ 30 cells were picked per replicate and RNA was extracted with PicoPure RNA Isolation Kit (Thermo Scientific, Cat# KIT0204) and cDNA was obtained with Ovation RNA-Seq system V2 (Nugen, Cat# 7102-32). qPCR analysis was performed using the SYBRGreen JumpStart Taq Ready-Mix Kit (Sigma, S4438) on Roche 480II qPCR machine. All primers for each gene were pretested using standard curve analysis; the amplification efficiency was found to be between 0.9 and 1.1. The detailed primer sequences are listed in Table S1. The cDNAs of samples passing qPCR quality control were fragmented using focused-ultrasonicator (Covaris, ME220 model). The final sequencing libraries were constructed via Ovation Rapid DR multiplex system (Nugen, Cat# 0319-32) and sequenced by Illumina Hiseq4000 platform. The raw data of RNA-Seq were deposited in NCBI SRA database with accession code: PRJNA544182.

2.5 | Transcriptome analysis between different cell populations

An average of 80 million reads were obtained per replicate. FastQC (v0.11.3) and Trimmomatic (v0.36) were used for quality control.[20] About 87% of reads were mapped to the mouse reference genome (GRCm38) with high quality, using STAR (v2.5.2b) with default parameters.[21] RSEM (v1.2.21) software was used to estimate the gene expression levels on the alignment file with default parameters. Gene abundances were presented in Transcript Per Million (TPM).[22] Differentially expressed genes were calculated based on raw counts using the HTSeq (v0.10.0) software.[23]

Besides our control wild-type glial cells (ID: #1, #2, and #3), new SGNs (ID: #4, #5, and #6) from experimental group-1 and new SGNs (ID: #7, #8, and #9) from experimental group-2, we also downloaded data from one previous SGN single-cell RNA-sequencing data.[4] This data were also generated by manual picking making it potentially comparable to our data. We re-analyzed the data and divided cells into four clusters based on results of t-SNE: Type I-A, Type I-B, Type I-C, and Type II (Figure 10), consistent with the original report of SGN subtypes.[4] We chose four samples, which were #372, #373, #365, and #452, to represent Type I-A, Type I-B, Type I-C, and Type II, respectively. These were distributed in the middle of their own clusters and should best represent global gene expression profiles of each cell type (Figure 10).

Initial cluster analysis suggested that new SGNs resembled Type I SGNs more than Type II. Therefore, we compared transcriptomes among our control wild-type glial cells (ID: #1, #2, and #3) and wild-type Type I SGNs (#372, #373, and #365), and chose the genes that showed significant differences between wild-type glial cells and SGNs (1927 genes). Next, we performed PCA analysis on these 1927 genes and looked at where the new SGNs from experimental group 1 and 2 were relative to the control cells. Functional enrichment analysis was performed by Metascape.[24]

3 | RESULTS

3.1 | Generating a new mouse line with inducible expression of Ngn1 and Neurod1

Transcription factors are widely used for cellular reprogramming.[25] *Neurog1* (also known as *Ngn1*) and *Neurod1* are b-HLH transcription factors that are necessary for SGN development.[26,27] In addition, Neurod1 is known to reprogram chromatin, induce neuronal gene expression, and is sufficient to successfully reprogram in vitro cochlear glial cells into SGNs which express neuronal markers, Tuj1, Map2, and Prox1.[15,28] We set out to induce ectopic *Ngn1* and *Neurod1* expression in neonatal cochlear glial cells in vivo via the Cre/Loxp-mediated genetic approach.[29]

We firstly constructed a new Cre-mediated conditional knock-in mouse strain, *Rosa26-CAG-Loxp-stop-Loxp-Neurog1*3xHA-P2A-Neurod1*3xFlag-T2A-EGFP*, which for short we called *Rosa26-LSL-Ngn1-Neurod1* (Figure

1A-C). Southern blot analysis confirmed that there was no random insertion (Figure 1D,E). By tail DNA PCR genotyping, wild type, heterozygous, and homozygous mice were easily identified (Figure 1F). If a *Rosa26-LSL-Ngn1-Neurod1* mouse is crossed with the glial cell specific *Plp1-CreER* mouse (to be described in details below), the double positive offspring would express polycistronic mRNA containing *Ngn1* (tagged with 3xHA), *Neurod1* (tagged with 3xFlag) and *EGFP* in glial cells upon exposure to tamoxifen (Figure 2A). Furthermore, fused protein (Ngn1-Neurod1-EGFP) was translated first, and individual protein was generated via 2A oligopeptide-mediated cleavage.[30] In addition, via this design, co-expression of Ngn1, Neurod1, and EGFP were guaranteed, which was confirmed by co-staining of EGFP with HA tag antibody (Figure 2B-D'') or Neurod1 antibody (Figure 2E-G''). We intended to stain Neurod1 with Flag antibody but failed to obtain good immunostaining signal. The nuclear expression of HA (Ngn1) and Neurod1 in EGFP+ cells occurred in a heterogeneous pattern (white arrows in Figure 2C-D'',F-G''). Surprisely, we also detected Neurod1+/EGFP− cells (yellow arrows in Figure 2E-G'') in both control and experimental groups, however, the Neurod1 distribution is membranous. It is possible that the Neurod1 antibody is not very specific or other cell types (i.e. blood vessel cells) did express Neurod1 in postnatal cochleae. Nonetheless, the permanent EGFP expression permitted lineage tracing and cell fate conversion analysis at a single-cell resolution as described below.

3.2 | Ectopic Ngn1 and Neurod1 can rapidly reprogram neonatal cochlear glial cells into SGNs within 6 days

To specifically induce ectopic Ngn1 and Neurod1 in neonatal cochlear glial cells, we used *Plp1-CreER* as the Cre driver

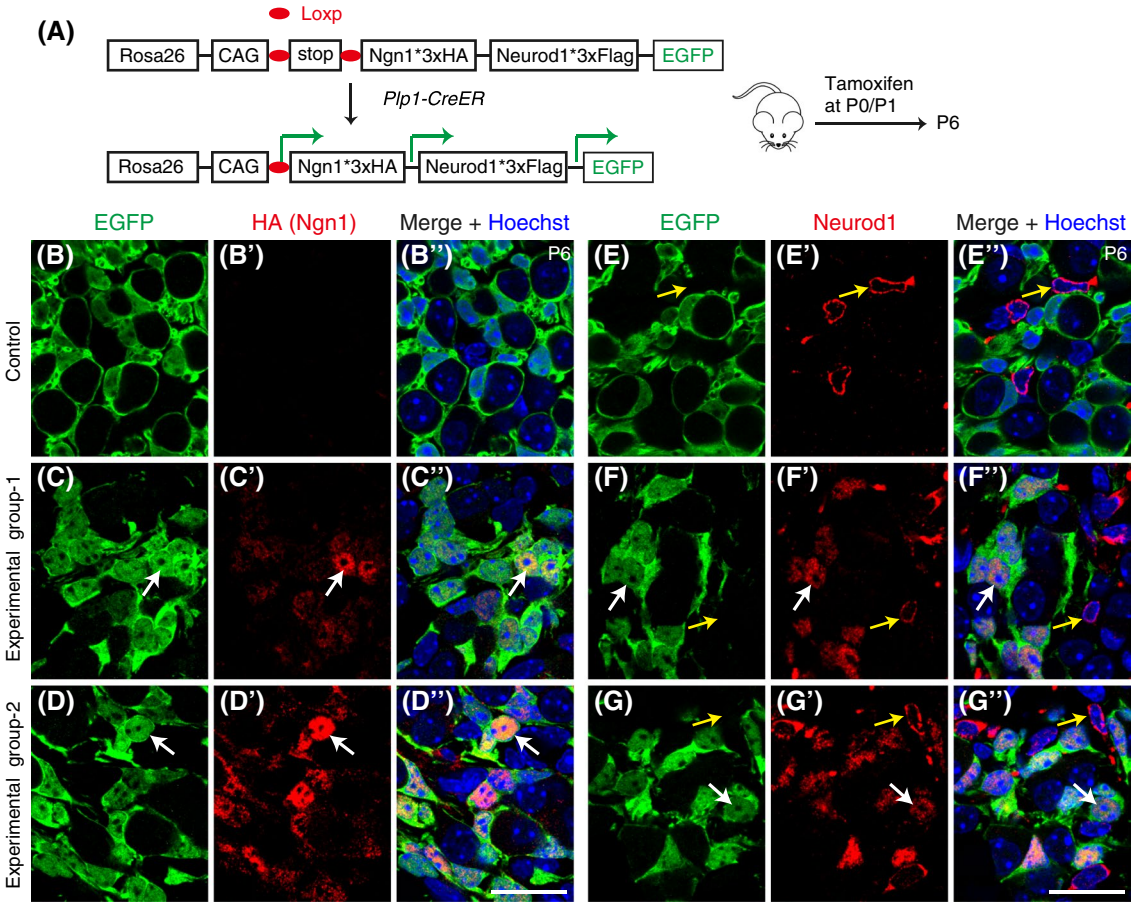

FIGURE 2 Ectopic expression of Ngn1 and Neurod1 in glial cells. A, Illustration of *Plp1-CreER* mediated removal of stop fragment and activation of Ngn1 and Neurod1. All tamoxifen injections were given at P0 and P1. B-D'', Co-staining of EGFP and HA in *Plp1-CreER+; Rosa26-CAG-LSL-3xEGFP (Ai47)/+* mice (control, B-B''), *Plp1-CreER+; Rosa26-LSL-Ngn1-Neurod1/+* (experimental group-1, C-C''), *Plp1-CreER+; Rosa26-LSL-Ngn1-Neurod1/Rosa26-LSL-Ngn1-Neurod1* (experimental group-2, D-D''). EGFP+ cells expressed Ngn1 in both experimental groups (white arrows in C-D'') but not in the control group. E-G'', Co-staining of EGFP and Neurod1 in the three groups. Again, EGFP+ cells with nuclear expression of Neurod1 were observed in experimental group-1 (white arrows in F-F'') and experimental group-2 (white arrows in G-G''), but not in control group (E-E''). Note that Neurod1 signal was detected in EGFP− cells in all three groups (yellow arrows in E-G''). The identity of these cells remains unclear. Scale bars: 20 μm

as it can label glial cells in postnatal cochlea, as reported in previous studies.[31,32] We also independently characterized *Plp1-CreER+; Rosa26-CAG-LSL-3xEGFP (Ai47)/+* mice (control group) that were given tamoxifen at postnatal day 0 (P0) and P1, and analyzed at P6. Cre-mediated EGFP expression overlapped with the glial marker Sox10 but not the neuronal marker Tuj1 (white arrows in Figure 3A-A'''). This confirmed the glial specific induction of Cre activity by *Plp1-CreER+*. Neither EGFP+/HA (Ngn1) + nor EGFP+/Neurod1+ cells were observed in control group (Figure 2B-B'',E-E''). EGFP+ cells in control group were wild-type glial cells, as demonstrated by overlapping Sox10 expression.

In contrast to the control group, EGFP+/Tuj1+ cells were present in abundance in the two different experimental groups that were also give tamoxifen at P0 and P1, and analyzed at P6 (white arrows in Figure 3B-C'''). The first group was *Plp1-CreER+; Rosa26-LSL-Ngn1-Neurod1/+* (one copy of *Ngn1* and *Neurod1)* and was called for short experimental

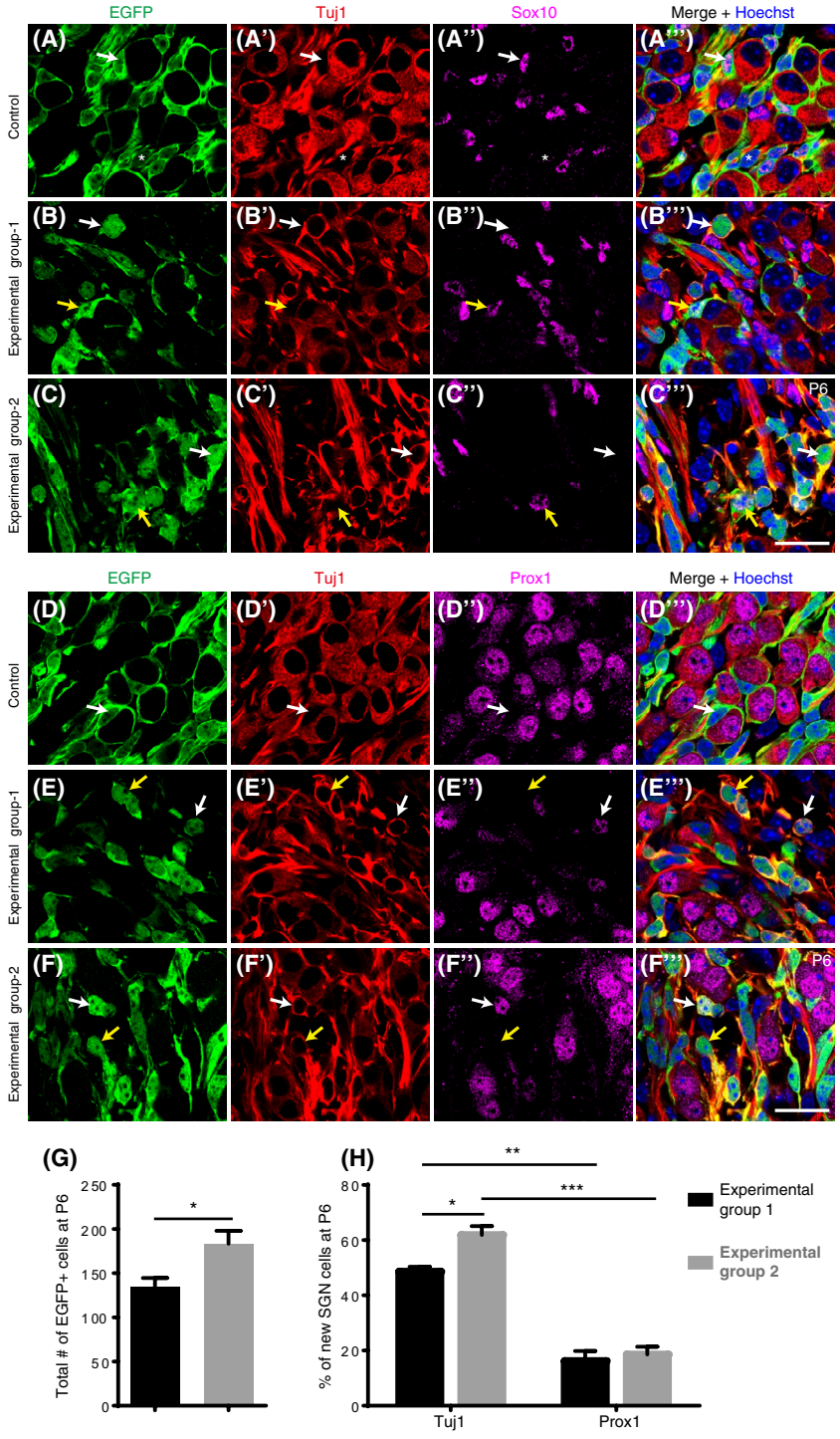

FIGURE 3 Glia-derived new SGNs turn on Tuj1 and Prox1 expression and reduce the glial marker Sox10 expression. A-C''', Triple staining of EGFP, Tuj1, and Sox10. Majority of EGFP+ cells expressed Sox10 but not Tuj1, confirming that they were indeed glial cells (white arrows in A-A'''). Note that a few EGFP+ glia cells expressed low or undetectable amounts of Sox10 (white stars in A-A'''), illustrating the fact that glial cells are heterogeneous. In contrast, EGFP+/Tuj1+ cells were observed in experimental group-1 and 2 (white arrows in B-C'''). These cells were defined as glial cells-derived new SGNs and also decreased glial marker Sox10 expression. Yellow arrows in (B-C''') pointed to EGFP+/Sox10+ cells which maintained glial phenotype and did not express Tuj1. D-F''', Triple staining of EGFP, Tuj1, and Prox1. Neither Tuj1 nor Prox1 was expressed in EGFP+ glial cells in the control (white arrows in D-D'''). Both EGFP+/Tuj1+/Prox1+ (white arrows in E-F''') and EGFP+/Tuj1+/Prox1- new SGNs (yellow arrows in E-F''') were observed in experimental group-1 and 2. G, Quantification of total EGFP+ cells (regardless of cell fates) per slide at P6. $*P < .05$. H, Percentage of new SGNs using different SGN marker (Tuj1 or Prox1) as a readout. $*P < .05$. $**P < .01$. $***P < .001$. Scale bars: 20 μm

group-1. The second group was *Plp1-CreER+; Rosa26-LSL-Ngn1-Neurod1/Rosa26-LSL-Ngn1-Neurod1* (two copies of *Ngn1* and *Neurod1)* and was named as experimental group-2. This demonstrated that upon Cre-mediated recombination, glial cells expressed EGFP, Ngn1, and Neurod1. Some of these cells also started expressing neuronal markers Tuj1; these were defined as glial lineage-derived new SGNs (new SGNs for short). Promisingly, most, if not all, of these new SGNs did not express Sox10 (white arrows in Figure 3B-C'''). We also observed EGFP+ cells that maintained Sox10 and did not express Tuj1 (yellow arrows in Figure 3B-C'''). These cells, which should be different from wild-type glial cells due to the induced Ngn1 and Neurod1 expression, were still defined as glial cells in our current study. Together, this suggested that Sox10 expression was repressed when neonatal glial cells were converted into SGNs.

Additional triple staining of EGFP, Tuj1, and Prox1 was performed. In control group, EGFP+ cells expressed neither Tuj1 nor Prox1 (white arrows in Figure 3D-D'''). However, EGFP+/Tuj1+/Prox1+ cells were observed in the two experimental groups (white arrows in Figure 3E-F'''). Intriguingly, we also captured cells that expressed EGFP and Tuj1 but not Prox1 (yellow arrows in Figure 3E-F'''). We did not observe cells that expressed EGFP and Prox1, but not Tuj1. This highlighted the variability in induction of neuronal gene expression in glia. Note that EGFP+ cells would be defined as new SGNs in our study, as long as they turned on one of the typical SGN markers. Because new SGNs were more frequently found in middle or apical turns at all ages (P6, P16 and P42) analyzed, we focused on them for the rest of the study.

Every tissue slice (~14 μm thickness) contained EGFP+ cells in the SGN region of the middle or apical cochlear turns. An average of 183.4 ± 8.4 EGFP+ cells were found in experimental group-2 at P6 (n = 3, mouse numbers); a smaller number was identified in experimental group-1 at P6, 135.0 ± 9.6 (n = 3, mouse numbers) (Figure 3G). Similarly, 61.9% ± 3.2% of the EGFP+ cells expressed Tuj1+ in experimental group-2, as compared to the lower 48.6% ± 1.8% found in experimental group-1 (Figure 3H). This suggested that two copies of *Ngn1* and *Neurod1* reprogrammed neonatal glial cells more efficiently into new SGNs than single copy. About 16.1% ± 3.6%, and 18.6% ± 2.8% of EGFP+ cells expressed Prox1 in experimental group-1 and group-2 at P6, respectively, (Figure 3H) and we did not see a statistically significant difference. Note that the cell body size of new SGNs were generally smaller than the surrounding wild-type SGNs (Prox1+/EGFP− or Tuj1+/EGFP−) in each group. We next wanted to assess how trans-differentiation of neonatal glia into new SGNs would progress as the animal aged, specifically focusing on the reprogramming efficiency and quality (i.e. the extent to which new SGNs resembled wild-type SGNs, and cell body morphology).

3.3 | New SGNs with large cell body were more frequently observed at P16

We analyzed cochlear samples from control and two experimental group mice that were given tamoxifen at P0/P1, and analyzed at P16 (Figure 4). Besides co-staining of EGFP with Tuj1 or Prox1 as described in Figure 3, we performed co-staining of EGFP and another neuronal marker Map2. In the control group, EGFP+ cells did not express Map2 (yellow arrows in Figure 4A-A''). In contrast, EGFP+/Map2+ cells were frequently observed in the two experimental groups (white arrows in Figure 4B-B'',C-C''). Again those cells were defined as new SGNs. A greater percentage of new SGNs with large and round nuclei (white arrows in Figure 4B-C'') were found at P16 than P6. More specifically, we found that EGFP+/Map2+ new SGNs always had larger cell bodies than EGFP+ cells that did not express Map2 and maintained as glial cells (compare white and yellow arrows in Figure 4B-C''). It suggested that, although those new SGNs were able to turn on Tuj1 or Prox1 as early as on P6 (Figure 3), those new SGNs may take ~16 days to be more differentiated and display large cell bodies.

Quantification analysis from multiple sections from three mice (either left or right ears) showed that 17.9 ± 0.7 (n = 3, mouse numbers) EGFP+ cells were found in experimental group-1 at P16, which was significantly smaller than the 31.6 ± 1.0 (n = 3, mouse numbers) found in experimental group-2 at P16 (Figure 4D). For each experimental group, the numbers of EGFP+ cells at P16 were lower than that found at P6 (compare Figures 3G and 4D), indicating that cell death likely occurred among EGFP+ cells between P6 and P16. Nevertheless, 54.1% ± 8.8% and 58.9% ± 8.4% of those EGFP+ cells were Tuj1+ (new SGNs) in experimental group-1 and 2, respectively; no significant difference was observed between two experimental groups (Figure 4E). 32.5% ± 5.6% of EGFP+ cells were Prox1+ in experimental group-1, which was slightly less than the 46.8% ± 2.0% found in experimental group-2 (Figure 4E). Lastly, 37.9% ± 6.8% and 51.7% ± 10.7% of EGFP+ cells were Map2+ in experimental group-1 and 2, respectively, and no significant difference was found (Figure 4E). Together, compared with new SGNs at P6, new SGNs displayed larger cell bodies and looked morphologically more like wild-type SGNs at P16. We picked new SGNs at P16 and performed RNA-Sequencing (RNA-Seq) analysis, as described below.

In addition, we determined whether fibers of those new SGNs were myelinated by the remaining glial cells (either EGFP+ or EGFP−). Myelin basic protein (Mbp) is one of three major myelin proteins and expressed in mouse SGN region.[33,34] Triple staining of EGFP, Mbp, and Prox1 showed that, similar to SGNs in control mice at P6 (arrows in Figure S1A-A''') and at P16 (arrows in Figure S1C-C'''), the new

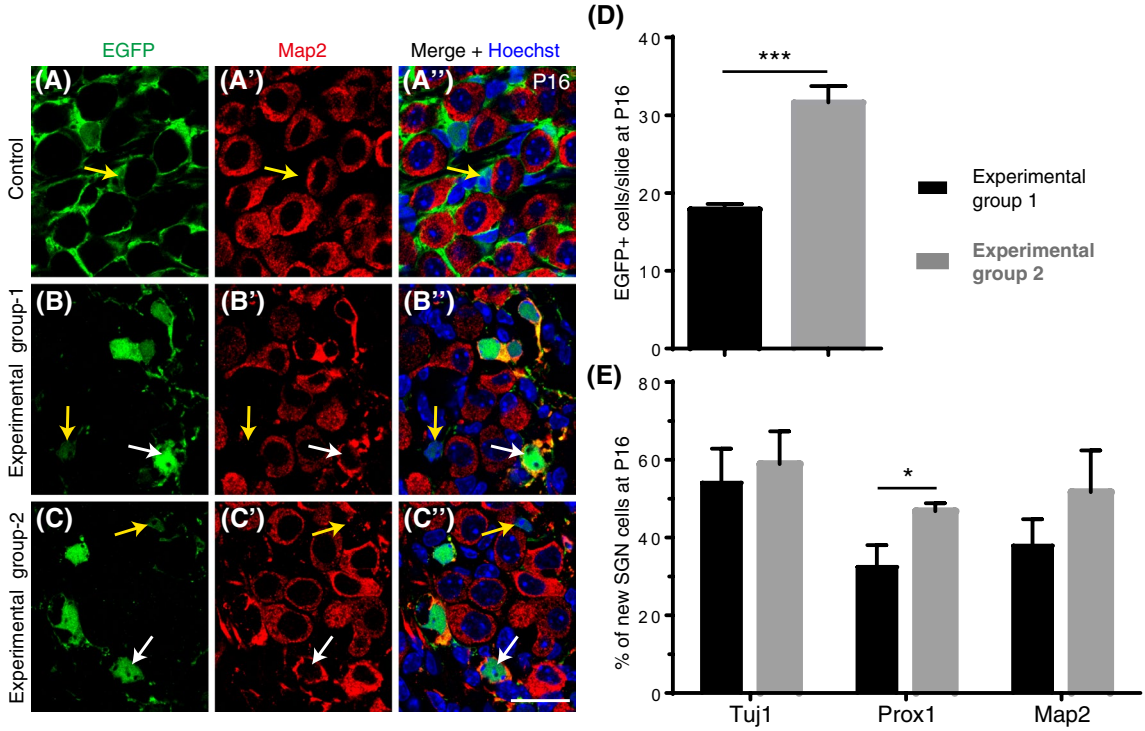

FIGURE 4 New SGNs also express Map2. A-C'', Double staining of EGFP and Map2, another SGN marker. EGFP+ cells did not express Map2 in control (yellow arrows in A-A''), but expressed Map2 in experimental group-1 and 2 (white arrows in B-C''). Yellow arrows in (B-C'') pointed to EGFP+ cells that did not express Map2 and kept glial cell fate. D, Quantification of the total number of EGFP+ cells (regardless of cell fates) per slide at P16. ***$P < .001$. E, Percentage of new SGNs using different SGN marker (Tuj1 or Prox1 or Map2) as a readout. *$P < .05$. The percentage of new SGNs in experimental group-2 tended to be higher than that in experimental group-1. A significant difference was only detected when using Prox1 as a readout. Scale bars: 20 μm

SGNs (EGFP+/Prox1+) in experimental group-2 mice were circled by the Mbp+ myelin sheath at P6 (arrows in Figure S1B-B''') and at P16 (arrows in Figure S1D-D'''). It supported that new SGNs were myelinated.

3.4 | New SGNs are still viable at P42

In addition to P6 and P16, we also analyzed new SGNs at P42. We analyzed cochlear samples dissected from mice at P42 that were given tamoxifen at P0/P1 (Figure 5). Similar to what we observed at P6 and P16, no EGFP+ cells expressed neuronal marker Map2 in the control group (yellow arrows in Figure 5A-A''). In contrast, new SGNs that co-expressed EGFP and Map2 were observed in experimental-1 (white arrows in Figure 5B-B'') and experimental-2 group (white arrows in Figure 5C-C''). Note that we observed multiple new SGNs with cell size and rounded morphology similar to that of the neighboring wild-type SGNs (Map2+/EGFP−) in experimental-2 group (white arrows in Figure 5C-C''). Again, EGFP+ cells, which did not express Map2, maintained as glial cell fate and displayed smaller cell bodies (yellow arrows in Figure 5B-C''). Quantitative analysis revealed that there were on average 20.9 ± 5.7 (n = 3, mouse numbers) EGFP+ cells in experimental group-1, and 18.3 ± 1.6 (n = 3, mouse numbers) EGFP+ cells in experimental group-2. No significant difference was present between the two experimental groups. Similar to P16, the total numbers of EGFP+ cells in both experimental groups were much less than those at P6 (Figure 5D). A significant difference was also observed when comparing the total number of EGFP+ cells in experimental group-2 at P16 and P42 (Figure 5D).

We next quantified the percentage of new SGNs among EGFP+ cells using different neuronal markers. We found that 6.7% ± 1.9% were Tuj1+ in experimental group-1, which was significantly less than 37.2% ± 6.0% in experimental group-2 (Figure 5E). Approximately, 12.7% ± 4.0% and 16.2% ± 6.0% were Prox1+ in experimental group-1 and 2, respectively, and there was no significant difference (Figure 5E). We found that 2.8% ± 0.8% were Map2+ in experimental group-1, which was significantly less than the 35.7% ± 7.9% found in experimental group-2 (Figure 5E). Together, this showed that new SGNs could survive at least until P42. Consistent with the observation at P6 (Figure 3H) and P16 (Figure 4E), two copies of Ngn1 and Neurod1 in experimental group-2 generally displayed a higher percentage of new SGNs than the single copy in experimental group-1 (Figure 5E). We further confirmed this Ngn1 and Neurod1 dosage-dependent effect on reprogramming efficiency using transcriptomic assays in the sections below.

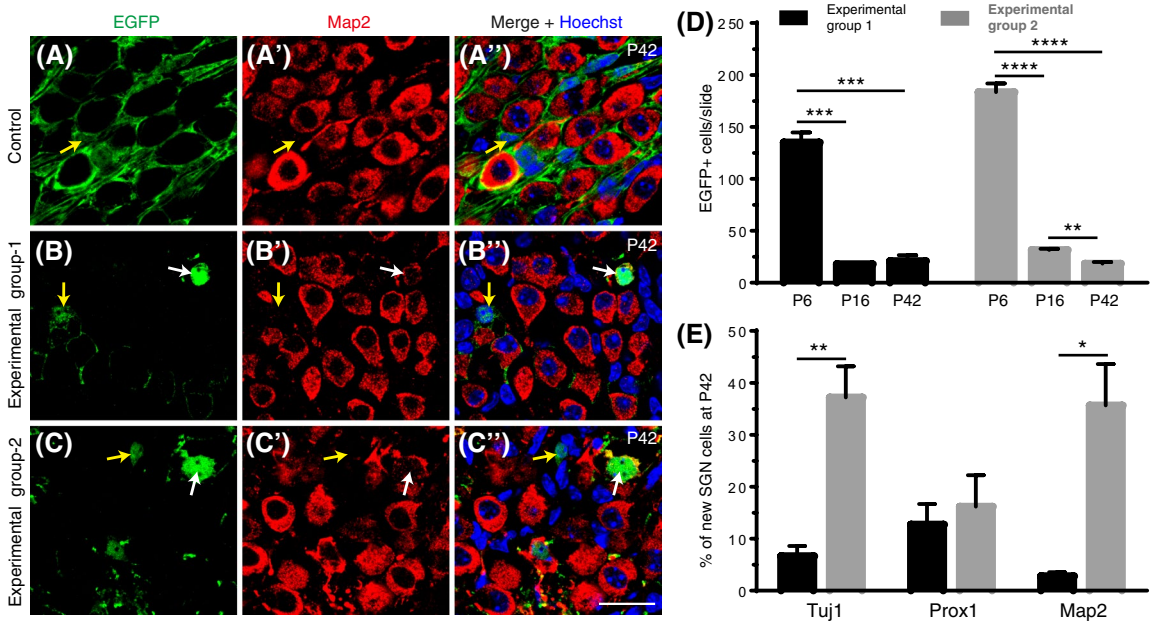

FIGURE 5 New SGNs can survive at least until P42. A-C'', Double staining of EGFP and Map2. Similar to P16 (Figure 4), there was no overlap between EGFP and Map2 in the control (yellow arrows in A-A''). However, EGFP+/Map2+ new SGNs were captured in experimental group-1 and 2 (white arrows in B-C''). Again, not all EGFP+ cells adopted SGN fate. Yellow arrows in (B-C'') pointed to EGFP+ cells that did not express Map2 and were defined as glial cells. Note that the cell body size of new SGNs was much larger than EGFP+/Map2- glial cells, especially in experimental group-2 (compare white and yellow arrows in C). D, Summary of the total number of EGFP+ cells (regardless of cell fates) per SGN region across all ages in two experimental groups at P42. $^{**}P < .01$, $^{***}P < .001$, $^{****}P < .0001$. The total numbers of EGFP+ cells at P16 and P42 were significantly smaller than those at P6. In addition, the number of EGFP+ cells also dropped significantly in experimental group-2 between P16 and P42. This was not observed in experimental group-1. E, Percentage of new SGNs using different SGN marker (Tuj1 or Prox1 or Map2) as a readout at P42 between the two experimental groups. A significant difference was found between experimental group-1 and 2 using Tuj1 and Map2 as readouts. $^{*}P < .05$. $^{**}P < .01$. Scale bars: 20 μm

3.5 | A small fraction of new SGNs express *Mafb* with cell size and morphology comparable to that of wild-type SGNs

We next aimed to determine whether the new SGNs which had larger and rounder cell bodies also expressed critical genes for SGN differentiation and function, such as *Mafb*. *Mafb* is required for SGN normal development; indeed, SGNs fail to form the normal ribbon synapses in *Mafb -/-* mice.[35] In control group, EGFP+/Tuj1+/Mafb+ cells were never observed (white arrows in Figure 6A-A''' and 7A-A'''). Although most of the EGFP+/Tuj1+ new SGNs failed to express Mafb (white arrows in Figure 6B-C'''), a few new SGNs did express Mafb (white arrows in Figure 7B-C'''). Quantification analysis showed that 5.70% ± 0.73% (n = 3, mouse numbers) and 4.22% ± 0.67% (n = 3, mouse numbers) of the new SGNs expressed Mafb in experimental group-1 and experimental group-2, respectively, and no statistically significant difference were observed at P16 (Figure 7D). As previously mentioned, the nuclei size of these EGFP+/Mafb+ cells was consistently comparable to neighboring wild-type SGNs. The presence of EGFP+/Mafb+ new SGNs was also confirmed by our transcriptomic analysis; see below for details.

3.6 | Transcriptome analysis confirms the heterogeneous nature of new SGNs

Our immunostaining assays described above demonstrated the cell fate conversion from neonatal glial cells into SGNs via ectopic *Ngn1* and *Neurod1*. We next wanted to compare the transcriptome of the different cell populations. To this end, we performed RNA-Seq on glial cells from control and new SGNs from two experimental groups. We manually picked EGFP+ cells from each group and pooled them together for per replicate at P16 (Figure 8A). We pooled cells and used bulk RNA-Seq, instead of single-cell RNA-Seq, because we aimed to cover more genes. Our qPCR analysis showed that *Ngn1*, *Neurod1,* and *Tuj1* were significantly enriched in cells from experimental groups, relative to those from control group (Figure 8B-D). In addition, *Ngn1* and *Tuj1* were much more highly expressed in experimental group-2 than that in experimental group-1. No significant differences were observed between two experimental groups with respect to *Neurod1*. We speculated that, besides the *Neurod1* expressed from the *Rosa26* loci, ectopic Ngn1 may turn on endogenous *Neurod1*. The initial qPCR analysis guaranteed the quality of cells that we manually picked.

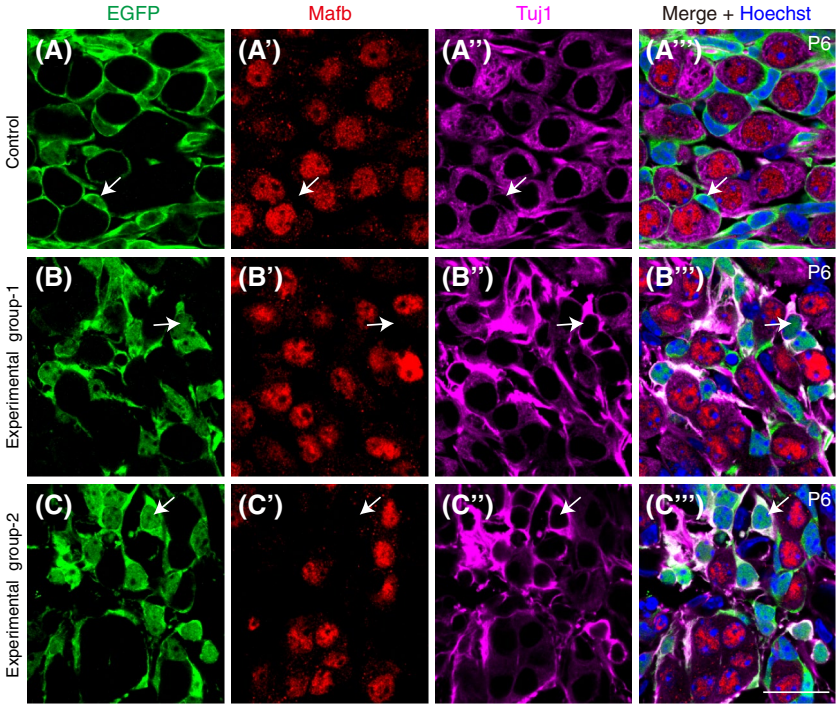

FIGURE 6 Majority of new SGNs do not express Mafb. Triple staining of EGFP, Tuj1 and Mafb in control (A-A'''), experimental group-1 (B-B'''), and experimental group-2 (C-C''') at P6. Neither Mafb nor Tuj1 was expressed in EGFP+ control glial cells (arrows in A-A'''). Many of the EGFP+ new SGNs expressed Tuj1 but not Mafb (arrows in B-C'''). A similar phenomenon was observed at P16 and P42 (not shown). Scale bars: 20 μm

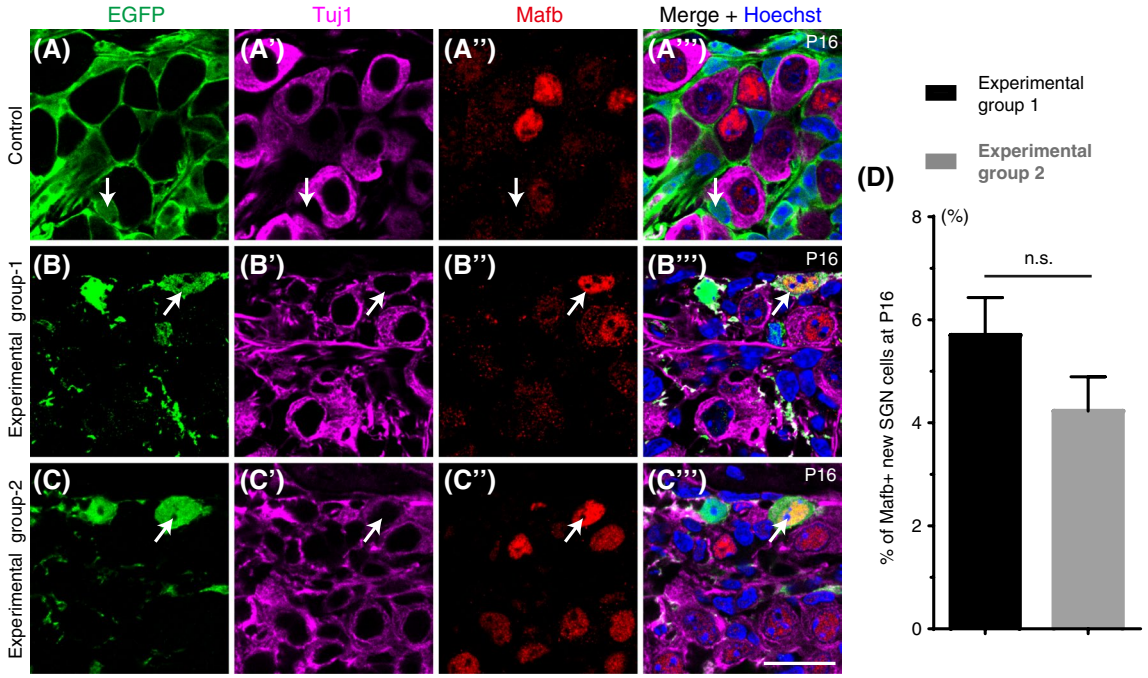

FIGURE 7 A small fraction of new SGNs express Mafb. Triple staining of EGFP, Tuj1 and Mafb at P16. A-A''', Similar to P6 (Figure 6), EGFP+ cells that did not express Tuj1 and Mafb were observed in control group. White arrows point to EGFP+/Tuj1-/Mafb- glial cells. B-C''', EGFP+/Tuj1+/Mafb+ new SGNs (white arrows in B-C''') were observed in both experimental groups. Intriguingly, their cell body size was large and comparable to neighboring wild-type EGFP−/Tuj1+ cells. D, Quantification of EGFP+/Mafb+ new SGNs at P16. Data were presented as Mean ± SEM. Scale bars: 20 μm

Samples of each group passing the qPCR quality control were further processed for RNA-Seq. Three replicates (~30 cells/replicate) were completed per group: control group (ID: #1, #2, and #3), experimental group-1 (ID: #4, #5, and #6), and experimental group-2 (ID: #7, #8, and #9). We first checked the expression of *Mafb*. The TPM (transcripts per million) value of *Mafb* in all glial cell samples from control group was zero (Figure 9A). In contrast, *Mafb* was detected in one out of three replicates in both experimental group-1 (#4, TPM = 5.11) and experimental group-2 (#9, TPM = 7.14)

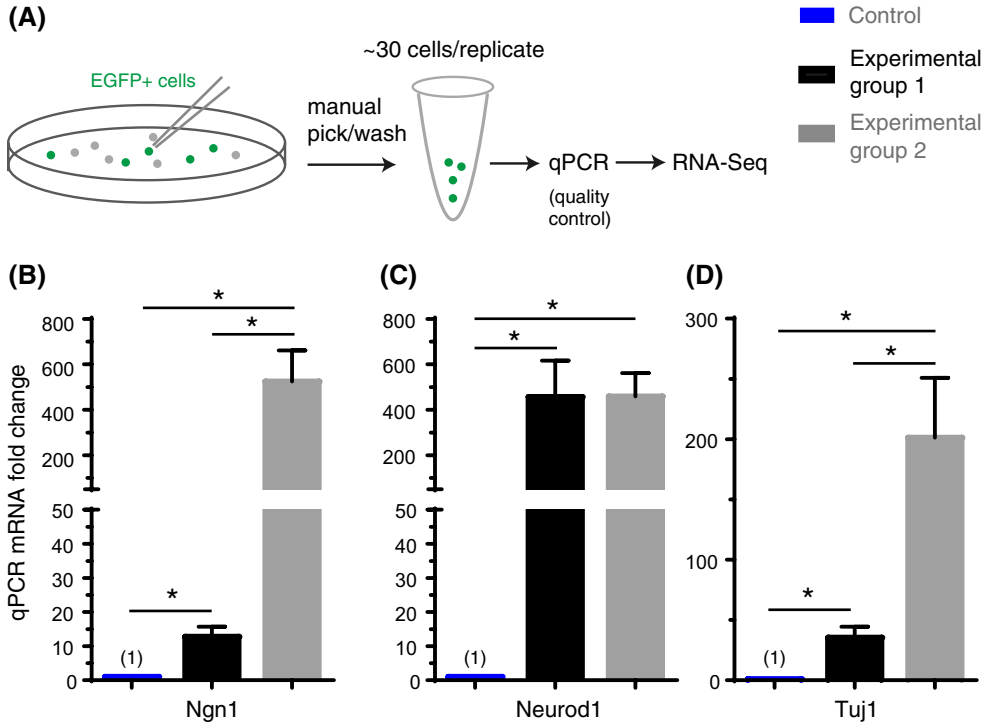

FIGURE 8 Manual cell picking and qPCR analysis of EGFP+ cells. A, Illustration of cell picking, qPCR quality control and RNA-Seq. EGFP+ cells from control and two experimental groups were picked. Per replicate, ~30 EGFP+ cells were collected in each group. B-D, qPCR analysis of three genes: *Ngn1* (B), *Neurod1* (C) and *Tuj1* (D). *y*-axis: fold change of mRNA in control, experimental group-1 and 2. The data were normalized to set the control value to be 1 for each gene. Compared to control, all genes were significantly more expressed in experimental groups. In addition, *Ngn1* and *Tuj1* also showed significant difference between experimental group-1 and 2. $*P < .05$

(red arrows in Figure 9A). To assess whether this was a chance detection or real signal, we further checked the expression of *Gata3* (Yu et al, 2013), a gene that is known to positively regulate *Mafb*, in samples #4 and #9. Gata3 was indeed also detected in samples #4 and #9 with a TPM value of 4.75 and 4.25, respectively (Figure 9B). Meanwhile, *Gata3* displayed no expression in all other samples (Figure 9B). Lastly, we also captured EGFP+ new SGNs that co-expressed Mafb and Gata3 at P16 (Figure 9C-C'''').

Although *Mafb* and *Gata3* were only significantly enriched in new SGNs of samples #4 and #9, *Tuj1* (*Tubb3*), *Prox1,* and *Map2* were, at different degrees, enriched in all the six samples (#4, #5, #6 and #7, #8, #9) of two experimental groups (green arrows in Figure 9D). It demonstrated that new SGNs were present in all the samples of experimental groups. In addition, we checked other SGN genes such as *Calb2, Pou4f1, Lypd1, Slc17a6, Slc17a7,* and *Pvalb*, which have recently been reported in different SGN single-cell RNA-Seq studies.[3-5] Samples #4 and #9 showed enhanced expression of all of these SGN genes compared to other samples (red arrows in Figure 9D). In parallel to this, there was a sharp drop in the expression of glia-related genes such as *Scn7a* in samples #4 and #9, as compared to the levels found in the control glia cells (#1, #2, and #3). Samples #5, #6, #7, and #8, in which *Mafb* and *Gata3* expression was low or undetectable, expressed intermediate levels of *Scn7a*. Taken together, the RNA-Seq analysis confirmed that EGFP+/Mafb+ new SGNs were better reprogrammed into SGN fate than those lacking Mafb expression. However, such cells were rare and only captured in two (#4 and #9) out of six samples from two experimental groups.

3.7 | Mafb+/Gata3+ new SGNs resemble wild-type I SGNs

We next specifically explored whether new SGNs from samples #4 and #9 resembled type I or type II SGNs. We downloaded a single-cell RNA-Seq dataset from a previous wild-type SGN single-cell study covering both type I and II SGNs, which was also performed via manual picking approach, and could serve as reference to score our new SGNs.[4] We were also able to divide the SGN single cells into four clusters (or cell types): Type I-A, Type I-B, Type I-C, and Type II (Figure 10A). One cell, which was located in the middle of each cluster, was picked to represent each cell type: Type I-A (#372), Type I-B (#373), Type I-C (#365), and Type II (#452). Those sample IDs were used according to the original report.[4] Hierarchical clustering analysis (HCA) showed that new SGNs from #4 and #9 resembled type I

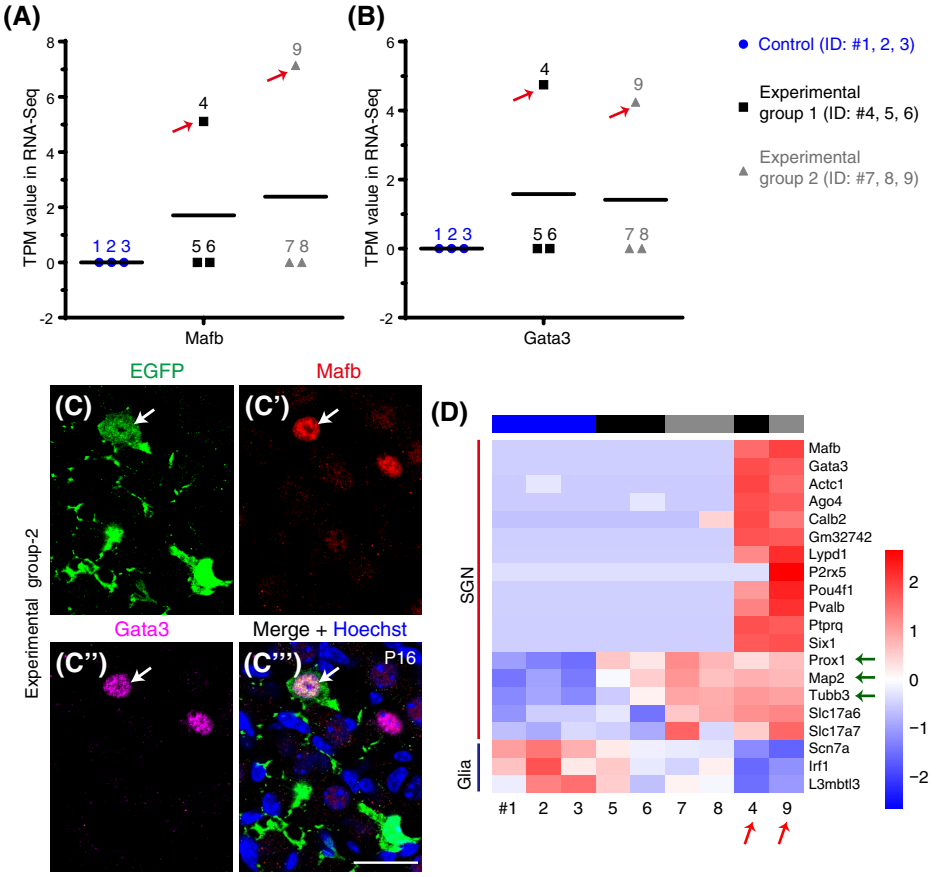

FIGURE 9 New SGNs expressing Mafb and Gata3 expression are better reprogrammed. A-B, Transcript per million (TPM) values of *Mafb* (A) and *Gata3* (B). Three replicates were included per group. Samples #4 (from experimental group-1) and #9 (from experimental group-2) contained new SGNs expressing *Mafb* and *Gata3*, while other samples did not. C-C''', Triple staining of EGFP, Mafb, and Gata3. Arrows point to EGFP+/Mafb+/Gata3+ new SGN. D, New SGNs from #4 and #9 (red arrows) show the most enrichment for SGN genes (red line, from Mafb to Slc17a7) as well as show lower expression of glial genes (blue line) such as *Scn7a*, *Irf1,* and *L3mbtl3*. Green arrows pointed to the neuronal markers, *Prox1*, *Map2,* and *Tuj1* (*Tubb3*), that we used to identify new SGNs

SGNs more than type II SGNs, as they were closer to each other (Figure 10B).

However, detailed computational analysis revealed that expression levels of 575 genes were significantly different ($P < .05$) among best reprogrammed new SGNs (#4 and #9) and type I SGNs (File S1). Those top differently expressed genes (i.e. *Nol11* and *Rrm2b*), and genes not significantly different (i.e. *Map7 and Mdp1*) were presented as examples in Figure 10C. It suggested that, although new SGNs from #4 and #9 were more similar to type I SGNs, additional factors are needed to further minimize their transcriptomic difference.

3.8 | Transcriptome analysis also supports that two copies of Ngn1 and Neurod1 results in better reprogramming of glial cells to SGNs than a single copy

To confirm the dosage-dependent effect of Ngn1 and Neurod1 on neonatal glial cells to SGN cell fate conversion, as supported by previous immunostaining assays (Figures 3-5), we further compared the transcriptome profiles between new SGNs from the two experimental groups and control glial cells. In total 1927 genes showed significantly differential expression among control glial cells (#1, #2, and #3) and three (#372, #373, and #365) Type I wild-type single SGNs. As illustrated in Figure 11A, principal component analysis (PCA) via those 1927 genes clearly divided cells into four clusters: control glial cells, type II SGNs, new SGNs, and Type I SGNs.

Apparently, new SGNs were closer to Type I SGNs than control glial cells (Figure 11A). Next, transcriptomic comparison was performed between control glial cells and new SGNs of experimental group-1 (#4, #5, #6), and experimental group-2 (#7, #8, #9), respectively. There were 87 upregulated, and 540 downregulated genes in SGNs of experimental group-1 (Figure 11B), and the full list of those 627 genes were summarized in File S2. In contrast, 368 genes were upregulated, and 867 were downregulated in new SGNs of experimental group-2 (Figure 11C), and the full list of those 1235 genes were summarized in File S3.

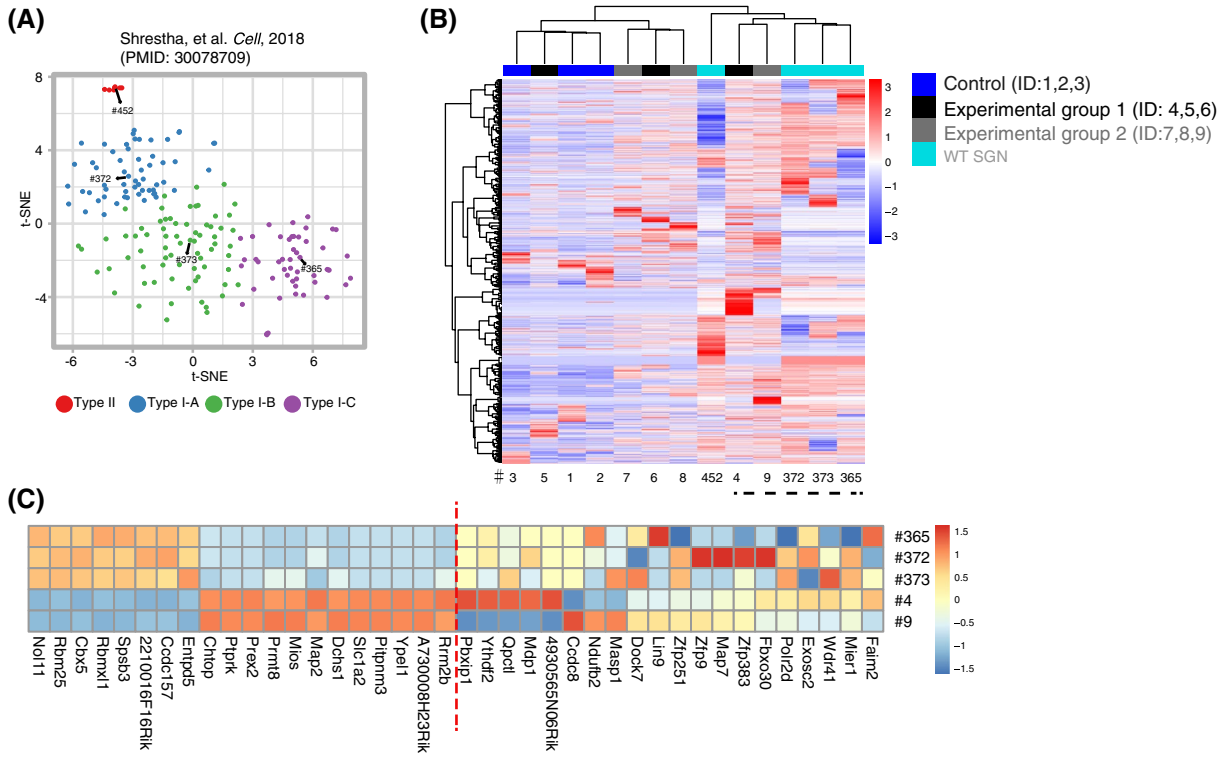

FIGURE 10 Mafb+/Gata3+ new SGNs are similar, but still different, to type I SGNs. A, Reanalysis of single-cell RNA-Seq data from a previous wild-type SGN single-cell RNA-Seq study. Four clusters were identified in results of the t-SNE analysis. Four cells, #372, #373, #365, and #452 which were located at the center of each cluster were selected to represent Type I-A, Type I-B, Type I-C, and Type II SGNs, respectively. B, Hierarchical clustering analysis showing that our new SGNs (from sample #4 and #9 in Figure 9) are closest to Type I SGNs (#372, #373, and #365). C, Exampled top differentially (left to red dotted line) and not differentially (right to red dotted line) expressed genes were presented

We additionally performed gene functional enrichment analysis on these differentially expressed genes and found that the 368 upregulated genes in the new SGNs of experimental group-2 were significantly enriched in neuron differentiation and neurotransmitter secretion pathway (red arrows in Figure 11C'). Consistently, Schwann cell differentiation genes were downregulated in new SGNs of both experimental group-1 and experimental group-2 (green arrows in Figure 11B'' and C''). Moreover, they were more significantly downregulated in experimental group-2. Together, these results supported that two copies of Ngn1 and Neurod1 overall could better reprogram glial cells into SGNs and activate more neuron differentiation genes, and simultaneously repress Schwann cell differentiation genes.

3.9 | Juvenile glial cells were insensitive to ectopic Ngn1 and Neurod1

Next we determined whether juvenile glial cells at 2 weeks old of age are responsive to ectopic Ngn1 and Neurod1. *Plp1-CreER+; Rosa26-CAG-LSL-3xEGFP (Ai47)/+* (control) and *Plp1-CreER+; Rosa26-LSL-Ngn1-Neurod1/Rosa26-LSL-Ngn1-Neurod1* (experimental group-2) mice were given tamoxifen at P14 and P15, and analyzed at P25. Numerous EGFP+ cells expressed Sox10 but not Tuj1 in control mice (white arrows in Figure 12A-A'''), confirming that they were glial cells. Unfortunately, we no longer observed the EGFP+/Tuj1+ cells in experimental group-2 mice. It supported that juvenile glial cells, different from neonatal glial cells, were insensitive to ectopic Ngn1 and Neurod1. Consistently, those EGFP+ cells maintained glial marker Sox10 (white arrows in Figure 12B-B'''). Such a declined reprogramming efficiency was also reported in *Ascl1*-mediated cell fate conversion from Müller glia to neurons in mouse retina after P16.[36]

3.10 | Neonatal cochlear supporting cells are normal with ectopic Ngn1 and Neurod1

Our previous study showed that cochlear SCs, primarily the inner phalangeal cells (IPhs) also could be targeted by the *Plp1-CreER+* strain.[37] Therefore, we determined whether ectopic *Ngn1* and *Neurod1* would also affect cell fate of IPhs. *Plp1-CreER+; Rosa26-CAG-LSL-3xEGFP (Ai47)/+* (control) and *Plp1-CreER+; Rosa26-LSL-Ngn1-Neurod1/+* (experimental group-1) mice were given tamoxifen at P0

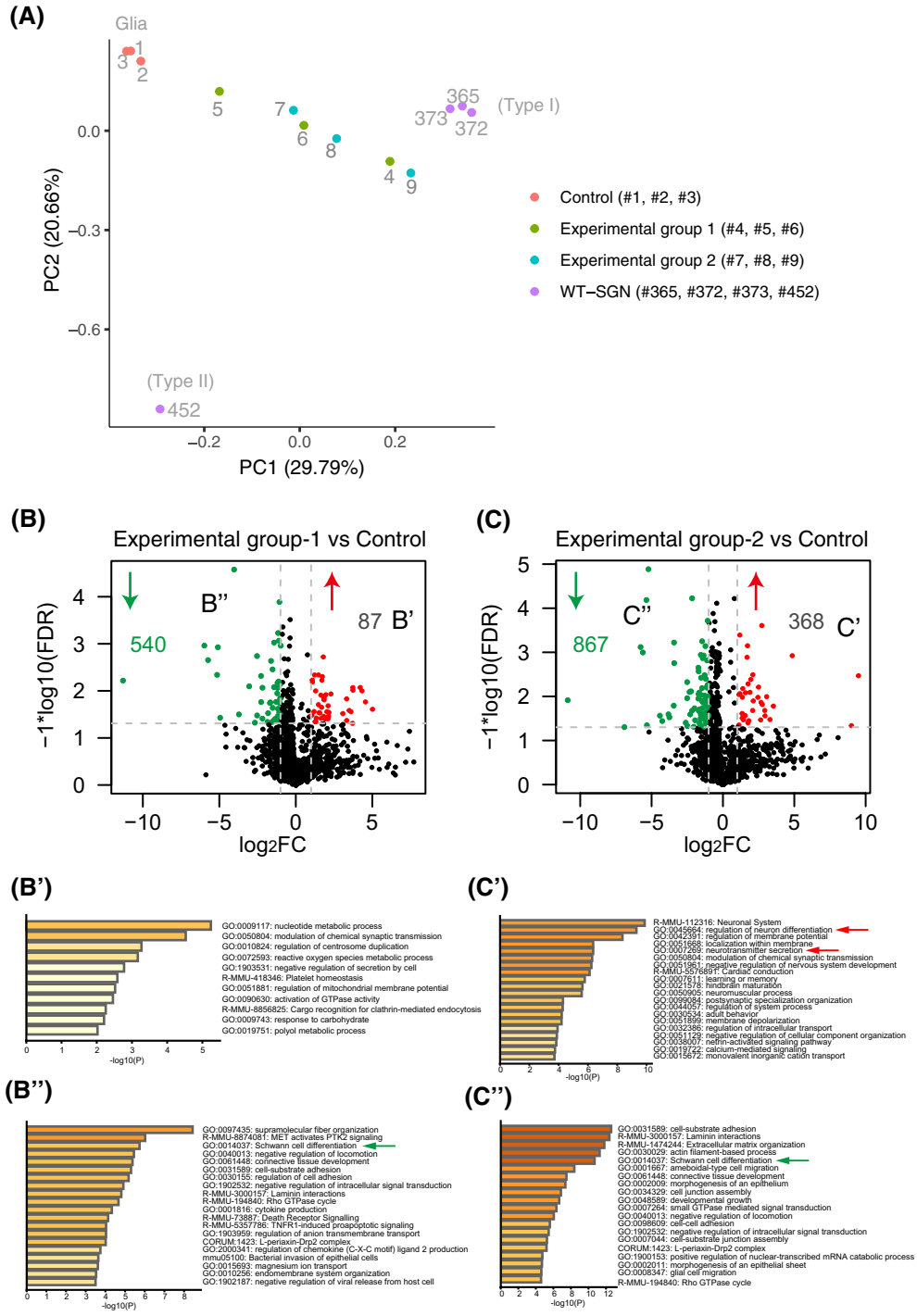

FIGURE 11 Dosage-dependent effects of Ngn1 and Neurod1 on reprogramming glial cells into SGNs. A, Principal component analysis (PCA) of new SGNs from experimental group-1 (#4, #5, and #6, single copy of *Ngn1* and *Neurod1*), experimental group-2 (#7, #8, and #9, two copies of *Ngn1* and *Neurod1*), wild-type glial cell populations (#1, #2, and #3), Type I-SGNs (#365, #372, #373), and Type II-SGN (#452). All new SGN populations were away from wild-type glial cells, supporting occurrence of cell fate change. B-C, volcano plots showing the most differentially expressed genes between new SGNs from experimental group-1 and glial cells from control (B), and new SGNs from experimental group-2 and glial cells from control (C). The *x*-axis indicates the log2 transformed fold change (FC) of genes between experimental groups and control, the *y*-axis represents the log10 transformed false discovery rate (FDR) value. Red and green dots represented genes that were significantly upregulated (red arrows) and downregulated (green arrows) between experimental group-1/2 and control, respectively, with the FC cutoff as 2 or ½, and FDR cutoff as 0.05. B'-C'', Functional enrichment analysis of upregulated (B' and C') and downregulated (B'' and C'') genes in Figure 11B and 11C. Red arrows in (C') pointed to upregulated gene families in new SGNs that are involved in neuron differentiation and neurotransmitter secretion. Green arrows (B'' and C'') pointed to genes that were downregulated and involved in Schwann cell differentiation. The degree of downregulation in (C'') was more than in (B'')

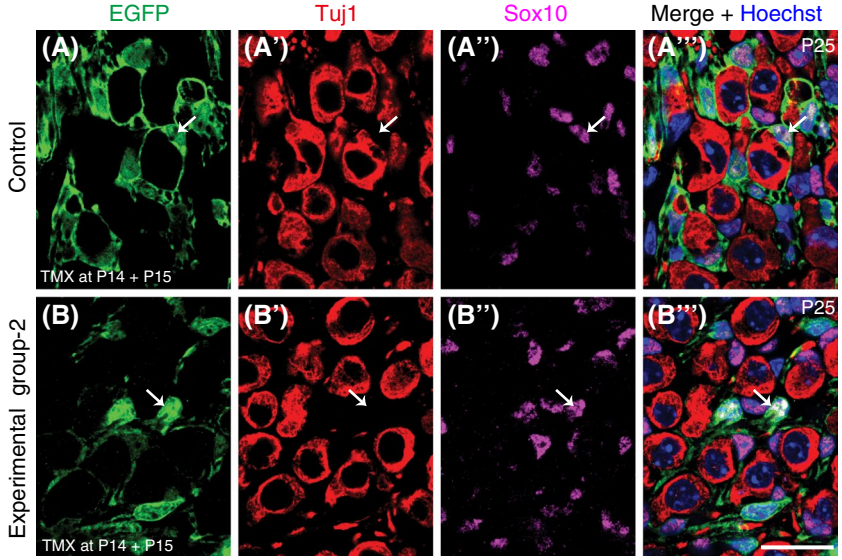

FIGURE 12 Ectopic Ngn1 and Neurod1 cannot convert juvenile glial cells into new SGNs. Triple staining of EGFP, Tuj1, and Sox10 in control (A-A''') and experimental group-2 mice (B-B''') that were both treated with tamoxifen at P14 and P15, and analyzed at P25. EGFP+ cells (arrows in A-A''') in control mice expressed Sox10 but not Tuj1, confirming their fate of glial cells. Different from observations in Figures 3-5, EGFP+ cells (arrows in B-B''') maintained Sox10 expression and failed to turn on Tuj1, supporting that they kept fate of glial cells and did not become SGNs. Scale bar: 20 μm

and P1, and analyzed at P6. In both control mice (Figure 13A-B''') and experimental group-1 mice (Figure 13C-D'''), EGFP+ IPhs did not express Map2 or Tuj1. Instead, they expressed SC marker Sox2 (arrows in Figure 13). EGFP+ IPhs were also Sox2+ when samples were analyzed at P16. Consistently, HCs were also normal in both groups. We additionally analyzed *Plp1-CreER+; Rosa26-LSL-Ngn1-Neurod1/Rosa26-LSL-Ngn1-Neurod1* (experimental group-2) mice and EGFP+ IPhs were Sox2+, too. Together, it suggested that cell fate of IPhs were still maintained even with ectopic Ngn1 and Neurod1 expression.

4 | DISCUSSION

In summary, our data showed that conditional induction of ectopic *Ngn1* and *Neurod1* reprogrammed cochlear neonatal glial cells into SGNs in vivo. The glial cells-derived new SGNs expressed multiple neuronal markers including Tuj1, Prox1, and Map2 as well as decreased glial markers *Sox10* and *Scn7a*. Although majority of the new SGNs failed to express Mafb and Gata3, a small population of new SGNs did, which was confirmed by both antibody staining and transcriptome assays. Intriguingly, Mafb+/Gata3+ new SGNs also expressed many other SGN genes including *Pou4f1*. *Pou4f1* positively regulates soma size of SGNs and also directly or indirectly controls IHC presynaptic calcium signaling.[38,39] As a consequence, those new SGNs always displayed a large cell body and round morphology, similar to wild-type Type I SGNs. Last, because EGFP signal was not strong enough to trace fibers of new SGNs, we could not address whether new SGNs could innervate HCs.

4.1 | Cochlear neonatal glia cells are plastic and can be reprogrammed into SGNs in situ

Previous studies showed that cochlear glia cells were plastic and could be converted into SGNs in vitro.[15] Our current study further demonstrated plasticity of neonatal glial cells in vivo. Our data supported that neonatal glial cells distributed in middle and apical cochlear turns were more plastic than those in basal turn (data not shown). Although cochlear glial cells has not been well studied yet, it is known that they can proliferate after damage.[40] This proliferative capacity may have advantages and it may help glial cells to repopulate, if some glial cells were converted to SGNs.

We also noticed that glial cells were heterogeneous in many aspects, as glial cells at least have two subtypes: Schwann cells and Satellite cells. SGN axons are myelinated by Schwann cells, and SGN cell bodies are wrapped by satellite cells.[31,32] Intriguingly, in control *Plp1-CreER+; Rosa26-CAG-LSL-3xEGFP (Ai47)/+* mice, majority of EGFP+ cells expressed glial marker Sox10, but we did observe a few EGFP+ cells with low or undetectable Sox10 (stars in Figure 3A-A'''), which suggested that glial cells were heterogeneous regarding Sox10 expression. In both experimental groups, EGFP+/Tuj1+ new SGNs diminished Sox10 expression (Figure 3B-C'''). Therefore, there were at least two explanations: one is that new SGNs decreased Sox10 during the

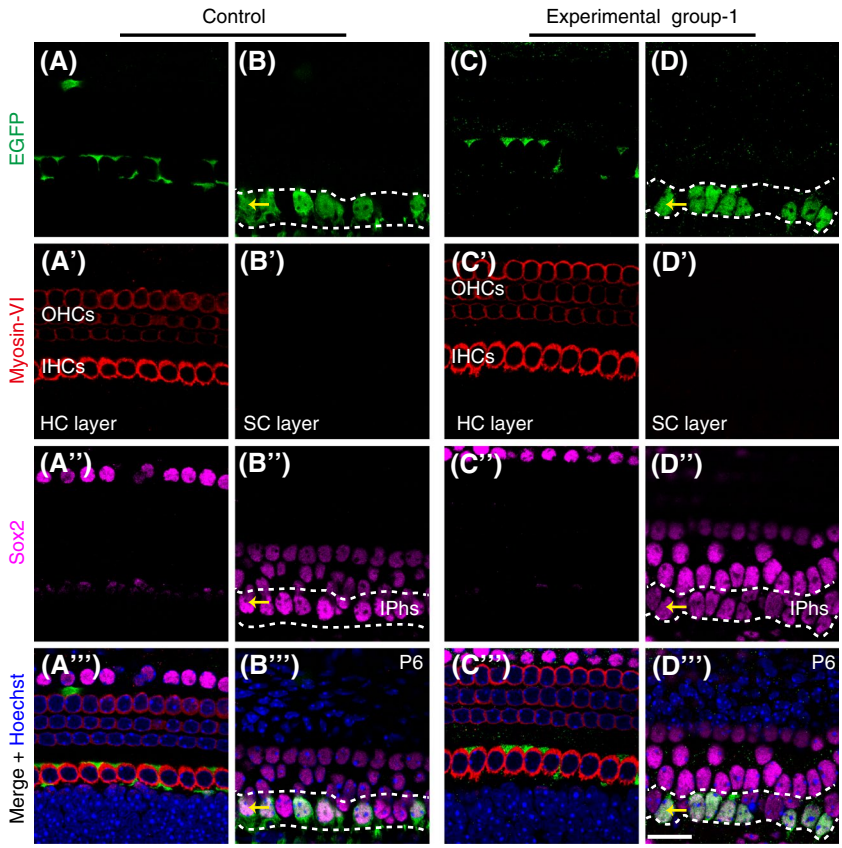

FIGURE 13 Cochlear supporting cells are normal in the presence of ectopic Ngn1 and Neurod1 at P6. A-B''', Cochlear samples of control mice were triple stained by EGFP, Myosin-VI, and Sox2 and scanned by confocal microscope at HC layer (A-A''') and SC layer (B-B'''). EGFP+ cells were primarily inner phalangeal cells (IPhs, yellow arrows in B-B''') below inner hair cells (IHCs). C-D''', Similarly, samples of experimental group-1 mice were triple stained by EGFP, Myosin-VI, and Sox2, and scanned at HC layer (C-C''') and SC layer (D-D'''). EGFP+ IPhs were Sox2+. Scale bar: 20 μm

reprogramming process; the other is that some new SGNs derived from neonatal glial cells that originally expressed low or undetectable Sox10.

4.2 | Multiple factors contribute to the heterogeneities of new SGNs

Our data clearly showed that new SGNs were heterogeneous (Figures 3H, 4E and 5E), suggesting that Tuj1 might be one of the earliest neuronal genes that new SGNs expressed. For instance, we observed new SGNs that expressed Tuj1 but not Prox1 (yellow arrows in Figure 3E-F'''). In addition, while the majority of new SGNs did not express Mafb (Figure 6), a small population of new SGNs expressed Mafb highly (Figure 7). Interestingly, Gata3 was also expressed in those EGFP/+Mafb+ new SGNs with large and rounded cell bodies (Figure 9), consistent with the requirement of *Gata3-Mafb* cascade during normal SGN development.[35] We speculated that once co-expression of Mafb and Gata3 was established in SGNs, this would act as a trigger inducing the expression of many other SGN genes, decreasing the expression of glial genes and leading the cells to display large rounded cell bodies akin to wild-type SGNs, as shown in Figure 9. Note that in this context Gata3 and Mafb should not be regarded as type II specific SGN marker, especially in those new SGNs, as these genes are expressed in both type I and II SGNs.[35,41] Similarly, *Pou4f1* is expressed in all SGNs at early embryonic ages but restricted to a subset of type I SGNs at adult ages.[38,39,42]

What could account for the heterogeneities of new SGNs? We provided two potential explanations. The first is that the heterogeneities are correlated with the original heterogeneous glial cells. It is possible that a small subset population of neonatal glial cells respond much better to ectopic Ngn1 and Neurod1 and are reprogrammed to SGN state with Mafb and Gata3 expression. The second is that reprogramming process itself is a stochastic process and there are various barriers at different steps, as also suggested by a recent Atoh1-mediated reprogramming of adult mouse utricle SCs into HCs.[43] We currently do not understand the mechanisms underlying the conversion of glial cells into SGN fate mediated by Ngn1 and Neurod1, nor how Ngn1 and Neurod1 regulate cell fate specification and differentiation in wild-type SGNs. Recently, it was reported that Ngn1 regulates CDK2 to promote proliferation in otic progenitors.[44]

Although we believe that the Mafb+ new SGNs might be able to partially function as wild-type SGNs, we cannot yet confirm this due to the current inability to identify Mafb+ new SGNs in alive tissues. To overcome this we plan on generating a *Mafb-P2A-tdtomato/+* knock-in mice to enable precise identification of the cells, allowing us to assess the electrophysiological properties of the rare Mafb+ new SGNs (EGFP+/tdtomato+) via patch-clamp recording in *Plp1-CreER+; Rosa26-LSL-Ngn1-Neurod1/Rosa26-LSL-Ngn1-Neurod1; Mafb-P2A-tdtomato/+* mice.

4.3 | Two copies of Ngn1 and Neurod1 shows higher reprogramming efficiency than one copy

Our quantification of results from the co-staining of EGFP and neuronal markers Tuj1, Prox1, and Map2 supported that two copies of *Ngn1* and *Neurog1* in experimental group-2 induced a higher reprogramming efficiency than a single copy of *Ngn1* and *Neurog1* in experimental group-1 (Figures 3H, 4E, and 5E). Consistently, our PCA analysis also suggested that the distance (or difference) between new SGNs from experimental group-2 and glial cells was larger than that between new SGNs from experimental group-1 and glial cells. Nonetheless, our data also showed that new SGNs from sample #4 (experimental group-1) and sample #9 (experimental group-2) were best reprogrammed. What could explain the reason that new SGNs from samples #7 and #8 (experimental group-2) were less reprogrammed than those in sample #4? We speculated that this seeming conflict was caused by the cell picking approach we used. EGFP+ cells were wild-type glial cells in control group, however, EGFP+ cells were either new SGNs or cells that maintained glial cell fates in the two experimental groups, as described above. We currently do not have the genetic model to exclusively select new SGNs. Instead, we tried our best to pick the EGFP+ cells with bigger and rounder nuclei, which would more likely be new SGNs according to our previous analysis at P16 (Figure 4). Glial genes *Sox10* and *Plp1* are highly expressed in glial cells, however, they did not show a significant difference among control and all experimental groups. Therefore, we proposed that our so-called new SGNs from two experimental groups, which were manually picked based on morphology and EGFP fluorescence, were mixed with a few glial cells. It is possible that the new SGNs from sample #4 (experimental group-1) had the least contaminations of EGFP+ glial cells, making new SGNs from sample #4 seem better reprogrammed than new SGNs from sample #7 and #8 (experimental group-2) that unfortunately had more contaminations of EGFP+ glial cells. Such glial contamination might reduce the sensitivity of our transcriptomic analysis, preventing us from thoroughly appreciating the dosage-dependent reprogramming effects of *Ngn1* and *Neurod1*. Last, it is possible that if we use transgenic, instead of knock-in approach, we might obtain multiple insertions of *Ngn1* and *Neurod1* transgene that would lead to higher Ngn1 and Neurod1 expression and better reprogramming efficiency.

4.4 | Regenerating SGNs in a mouse model with prior degeneration

The primary aim of our current pilot study was to demonstrate the plasticity of glial cells which, upon ectopic *Ngn1* and *Neurod1*, can be reprogrammed into SGNs. Note that our current model did not include any cochlear SGN degeneration prior to turning on Ngn1 and Neurod1 at P0/P1. It remains to be seen whether prior SGN death might promote Ngn1 and Neurod1-mediated glial cell to SGN fate conversion or increase the numbers of Mafb+ new SGNs. Ouabain, a potent inhibitor of Na^+/K^+-ATPase pump, can trigger degeneration of SGNs at adult mammalian cochlea.[45,46] We are not aware of any studies using ouabain in neonatal cochlea in vivo. If ouabain is toxic to neonatal mice, we plan on generating a genetic mouse model such as *Lypd1-P2A-DTR/+* to conditionally induce cell death of Lypd1+ SGNs, as SGN subtypes expressing Lypd1 are more vulnerable to degenerate in aged mice.[4] Diphtheria toxin (DT) treatment will trigger binding of DT with Diphtheria toxin receptor (DTR) and turn on a signaling cascade leading to cell death. This would be a promising model to mimic human aging-related SGN degeneration. Based on this model, we could further test whether combinational induction of *Ngn1, Neurod1,* and other factors (i.e. *Mafb* and *Gata3*) in glial cells will regenerate functional SGNs.

ACKNOWLEDGMENT

We thank Dr Qian Hu and the Optical Imaging Facility from the Institute of Neuroscience for support on image analysis. Dr Virginia M. S. Rutten, HHMI-Janelia Research Campus (Ashburn, VA, USA) for assistance in editing the text. The *Rosa26-LSL-Ngn1-Neurod1/+* strain knock-in mouse was generated by Beijing Biocytogen Co., ltd. This research is supported by National Key R&D Program of China (2017YFA0103901), Strategic Priority Research Program of Chinese Academy of Science (XDB32060100), Chinese Thousand Young Talents Program, National Natural Science Foundation of China (81771012), Shanghai Municipal Science and Technology Major Project (2018SHZDZX05), Innovative research team of high-level local universities in shanghai and the Faculty Research Award from Boehringer Ingelheim (BI) International GmbH (DE811138149).

CONFLICT OF INTEREST

The authors declare no conflicts of interest.

AUTHOR CONTRIBUTIONS

Z. Liu performed design and conceptualization. Z. Liu, X. Li, Z. Bi, and Y. Sun wrote the paper. X. Li, Z. Bi, and C. Li performed experiment and analyzed data. Y. Sun and Y. Li contributed analysis tools.

REFERENCES

1. Kelley MW. Regulation of cell fate in the sensory epithelia of the inner ear. *Nat Rev Neurosci*. 2006;7:837-849.
2. Li C, Shu Y, Wang G, et al. Characterizing a novel vGlut3-P2A-iCreER knockin mouse strain in cochlea. *Hear Res*. 2018;364:12-24.

3. Sun S, Babola T, Pregernig G, et al. Hair cell mechanotransduction regulates spontaneous activity and spiral ganglion subtype specification in the auditory system. *Cell*. 2018;174:1247-1263.e15.
4. Shrestha BR, Chia C, Wu L, Kujawa SG, Liberman MC, Goodrich LV. Sensory neuron diversity in the inner ear is shaped by activity. *Cell*. 2018;174:1229-1246.e17.
5. Petitpre C, Wu H, Sharma A, et al. Neuronal heterogeneity and stereotyped connectivity in the auditory afferent system. *Nat Commun*. 2018;9:3691.
6. Barclay M, Ryan AF, Housley GD. Type I vs type II spiral ganglion neurons exhibit differential survival and neuritogenesis during cochlear development. *Neural Dev*. 2011;6:33.
7. Froud KE, Wong AC, Cederholm JM, et al. Type II spiral ganglion afferent neurons drive medial olivocochlear reflex suppression of the cochlear amplifier. *Nat Commun*. 2015;6:7115.
8. Kujawa SG, Liberman MC. Adding insult to injury: cochlear nerve degeneration after "temporary" noise-induced hearing loss. *J Neurosci*. 2009;29:14077-14085.
9. Nishimura K, Weichert RM, Liu W, Davis RL, Dabdoub A. Generation of induced neurons by direct reprogramming in the mammalian cochlea. *Neuroscience*. 2014;275:125-135.
10. Wise AK, Tu T, Atkinson PJ, et al. The effect of deafness duration on neurotrophin gene therapy for spiral ganglion neuron protection. *Hear Res*. 2011;278:69-76.
11. Schmiedt RA, Okamura HO, Lang H, Schulte BA. Ouabain application to the round window of the gerbil cochlea: a model of auditory neuropathy and apoptosis. *J Assoc Res Otolaryngol*. 2002;3:223-233.
12. Chen W, Jongkamonwiwat N, Abbas L, et al. Restoration of auditory evoked responses by human ES-cell-derived otic progenitors. *Nature*. 2012;490:278-282.
13. Nishimura K, Nakagawa T, Sakamoto T, Ito J. Fates of murine pluripotent stem cell-derived neural progenitors following transplantation into mouse cochleae. *Cell Transplant*. 2012;21:763-771.
14. Guo Z, Zhang L, Wu Z, Chen Y, Wang F, Chen G. In vivo direct reprogramming of reactive glial cells into functional neurons after brain injury and in an Alzheimer's disease model. *Cell Stem Cell*. 2014;14:188-202.
15. Noda T, Meas SJ, Nogami J, et al. Direct reprogramming of spiral ganglion non-neuronal cells into neurons: toward ameliorating sensorineural hearing loss by gene therapy. *Front Cell Dev Biol*. 2018;6:16.
16. Loffler K, Schafer P, Volkner M, Holdt T, Karl MO. Age-dependent Muller glia neurogenic competence in the mouse retina. *Glia*. 2015;63:1809-1824.
17. Yao K, Qiu S, Wang YV, et al. Restoration of vision after de novo genesis of rod photoreceptors in mammalian retinas. *Nature*. 2018;560:484-488.
18. Li X, Yu B, Sun Q, et al. Generation of a whole-brain atlas for the cholinergic system and mesoscopic projectome analysis of basal forebrain cholinergic neurons. *Proc Natl Acad Sci U S A*. 2018;115:415-420.
19. Liu Z, Owen T, Zhang L, Zuo J. Dynamic expression pattern of Sonic hedgehog in developing cochlear spiral ganglion neurons. *Dev Dyn*. 2010;239:1674-1683.
20. Bolger AM, Lohse M, Usadel B. Trimmomatic: a flexible trimmer for Illumina sequence data. *Bioinformatics*. 2014;30:2114-2120.
21. Dobin A, Davis CA, Schlesinger F, et al. STAR: ultrafast universal RNA-seq aligner. *Bioinformatics*. 2013;29:15-21.
22. Li B, Dewey CN. RSEM: accurate transcript quantification from RNA-Seq data with or without a reference genome. *BMC Bioinformatics*. 2011;12:323.
23. Anders S, Pyl PT, Huber W. HTSeq—a Python framework to work with high-throughput sequencing data. *Bioinformatics*. 2015;31:166-169.
24. Zhou Y, Zhou B, Pache L, et al. Metascape provides a biologist-oriented resource for the analysis of systems-level datasets. *Nat Commun*. 2019;10:1523.
25. Takahashi K, Yamanaka S. A decade of transcription factor-mediated reprogramming to pluripotency. *Nat Rev Mol Cell Biol*. 2016;17:183-193.
26. Ma Q, Anderson DJ, Fritzsch B. Neurogenin 1 null mutant ears develop fewer, morphologically normal hair cells in smaller sensory epithelia devoid of innervation. *J Assoc Res Otolaryngol*. 2000;1:129-143.
27. Liu M, Pereira FA, Price SD, et al. Essential role of BETA2/NeuroD1 in development of the vestibular and auditory systems. *Genes Dev*. 2000;14:2839-2854.
28. Pataskar A, Jung J, Smialowski P, et al. NeuroD1 reprograms chromatin and transcription factor landscapes to induce the neuronal program. *EMBO J*. 2016;35:24-45.
29. Cox BC, Liu Z, Lagarde MM, Zuo J. Conditional gene expression in the mouse inner ear using Cre-loxP. *J Assoc Res Otolaryngol*. 2012;13:295-322.
30. Ryan MD, Drew J. Foot-and-mouth disease virus 2A oligopeptide mediated cleavage of an artificial polyprotein. *EMBO J*. 1994;13:928-933.
31. Wan G, Corfas G. Transient auditory nerve demyelination as a new mechanism for hidden hearing loss. *Nat Commun*. 2017;8:14487.
32. Gomez-Casati ME, Murtie J, Taylor B, Corfas G. Cell-specific inducible gene recombination in postnatal inner ear supporting cells and glia. *J Assoc Res Otolaryngol*. 2010;11:19-26.
33. Knipper M, Bandtlow C, Gestwa L, et al. Thyroid hormone affects Schwann cell and oligodendrocyte gene expression at the glial transition zone of the VIIIth nerve prior to cochlea function. *Development*. 1998;125:3709-3718.
34. Xing Y, Samuvel DJ, Stevens SM, Dubno JR, Schulte BA, Lang H. Age-related changes of myelin basic protein in mouse and human auditory nerve. *PLoS ONE*. 2012;7:e34500.
35. Yu WM, Appler JM, Kim YH, Nishitani AM, Holt JR, Goodrich LV. A Gata3-Mafb transcriptional network directs post-synaptic differentiation in synapses specialized for hearing. *Elife*. 2013;2:e01341.
36. Jorstad NL, Wilken MS, Grimes WN, et al. Stimulation of functional neuronal regeneration from Muller glia in adult mice. *Nature*. 2017;548:103-107.
37. Liu Z, Fang J, Dearman J, Zhang L, Zuo J. In vivo generation of immature inner hair cells in neonatal mouse cochleae by ectopic Atoh1 expression. *PLoS ONE*. 2014;9:e89377.
38. Huang EJ, Liu W, Fritzsch B, Bianchi LM, Reichardt LF, Xiang M. Brn3a is a transcriptional regulator of soma size, target field innervation and axon pathfinding of inner ear sensory neurons. *Development*. 2001;128:2421-2432.
39. Sherrill HE, Jean P, Driver EC, et al. Pou4f1 defines a subgroup of Type I spiral ganglion neurons and is necessary for normal inner hair cell presynaptic Ca(2+) signaling. *J Neurosci*. 2019;39:5284-5298.
40. Lang H, Li M, Kilpatrick LA, et al. Sox2 up-regulation and glial cell proliferation following degeneration of spiral ganglion

neurons in the adult mouse inner ear. *J Assoc Res Otolaryngol*. 2011;12:151-171.
41. Nishimura K, Noda T, Dabdoub A. Dynamic expression of Sox2, Gata3, and Prox1 during primary auditory neuron development in the mammalian cochlea. *PLoS ONE*. 2017;12:e0170568.
42. Deng M, Yang H, Xie X, Liang G, Gan L. Comparative expression analysis of POU4F1, POU4F2 and ISL1 in developing mouse cochleovestibular ganglion neurons. *Gene Expr Patterns*. 2014;15:31-37.
43. Jen HI, Hill MC, Tao L, et al. Transcriptomic and epigenetic regulation of hair cell regeneration in the mouse utricle and its potentiation by Atoh1. *Elife*. 2019;8:e44328.
44. Song Z, Jadali A, Fritzsch B, Kwan KY. NEUROG1 regulates CDK2 to promote proliferation in otic progenitors. *Stem Cell Reports*. 2017;9:1516-1529.
45. Yuan Y, Shi F, Yin Y, et al. Ouabain-induced cochlear nerve degeneration: synaptic loss and plasticity in a mouse model of auditory neuropathy. *J Assoc Res Otolaryngol*. 2014;15:31-43.
46. Lang H, Schulte BA, Schmiedt RA. Ouabain induces apoptotic cell death in type I spiral ganglion neurons, but not type II neurons. *J Assoc Res Otolaryngol*. 2005;6:63-74.

SUPPORTING INFORMATION

Additional supporting information may be found online in the Supporting Information section.

How to cite this article: Li X, Bi Z, Sun Y, Li C, Li Y, Liu Z. In vivo ectopic Ngn1 and Neurod1 convert neonatal cochlear glial cells into spiral ganglion neurons. *The FASEB Journal*. 2020;00:1–19. https://doi.org/10.1096/fj.201902118R